UNIVERSITY OF CALIFORNIA,
IRVINE

Synthesis and Surface Modification of Colloidal Germanium and Germanium-based Nanocrystals for Bottom-up Assembly of Nanostructured Thin Films

THESIS

submitted in partial satisfaction of the requirements
for the degree of

MASTER OF SCIENCE

in Chemistry

by

Torin Joseph Dupper

Thesis Committee:
Professor Allon I. Hochbaum, Chair
Professor Matthew D. Law
Professor Reginald M. Penner

2018

DEDICATION

To

my family and friends

who keep me happy

TABLE OF CONTENTS

LIST OF FIGURES

LIST OF TABLES

ACKNOWLEDGMENTS

First, I would like to thank Professor Allon Hochbaum for who took me into his group and providing a laboratory space for me to learn and work. I have developed as a scientist during my time in the lab, and I have gained a greater appreciation and interest for nanomaterial research.

I would also like to thank all of my fellow colleagues in Professor Hochbaum's lab. Thank you to Arunima and Nicole, especially, for keeping me sane and making the down time in lab fun and relaxing.

Finally, I would like to thank my professors and colleagues from other labs. Especially, the Rupert lab, Shea lab, and Law lab. I have learned a lot from everyone here at UCI, and I am happy that I was afforded the opportunity to work and learn here.

ABSTRACT OF THE THESIS

Synthesis and Surface Modification of Colloidal Germanium and Germanium-based Nanocrystals for Bottom-up Assembly of Nanostructured Thin Films

By

Torin Joseph Dupper

Master of Science in Chemistry

University of California, Irvine, 2018

Professor Allon I. Hochbaum, Chair

The colloidal synthesis and surface modification of germanium and germanium-based nanomaterials is a developing area of research with potential applications in a variety of fields. Colloidal germanium nanocrystal syntheses have improved significantly in recent years, but there has been little exploration into the synthesis of Ge-based nanomaterials, especially metal-germanium nanocrystals. A solution-phase synthesis of nickel germanide nanocrystals was developed to produce colloidal particles possessing an unexpected $Ni_{19}Ge_{12}$ crystal phase. The mechanism of this synthesis was explored to show that the $Ni_{19}Ge_{12}$ phase formed over a wide range of experimental conditions, but the use of a trioctylphosphine cosolvent allowed formation of a Ni_1Ge_1 phase that was not thermally stable. Many proposed applications of colloidal Ge nanocrystals require thorough particle surface modification. To this end, surface ligand exchange of Ge nanocrystals was examined and improved through the development of a high-temperature sulfur treatment. Finally, Ge nanocrystal films were cast from solution and their electrical conductivity was characterized.

Chapter 1: Introduction and Background

Germanium and Ge-based nanomaterials have been long been an attractive candidate for applications in optoelectronics, energy conversion, and bioimaging.[1–4] Germanium is environmentally friendly, has a small bandgap (0.67 eV) and a large Bohr radius (~ 24 nm), and possesses favorable electronic transport properties.[5] Thus, methods for the synthesis, modification, and processing of germanium nanomaterials are desirable to address technological needs in a variety of fields.

1.1 The Case for Heterostructured Thermoelectric Nanomaterials

As global energy consumption continues to rise, technological advances in renewable energy are necessary to limit the environmental impact of fossil fuels. Fossil fuels are estimated to produce 90% of the world's energy, which lose about 60% of released energy as waste heat and totaling ~40 PWh of wasted energy per year.[6] Thermoelectric (TE) materials can convert heat into electricity and could recycle the abundance of wasted thermal energy into usable electricity. Even modest recapture of this waste heat would greatly enhance the efficiencies of burning fossil fuel, but commercial TE devices are limited to niche applications by their raw material and processing costs.[7,8] Despite recent advances in the field, further improvements are necessary for widespread use of TE devices.[7]

The Thermoelectric Effect

When a temperature gradient is applied across a material, the transport of heat by charge carriers from the hot to the cold side creates an electric potential, which can drive an external load. The efficiency of TE devices, η, is a function of the Carnot efficiency, $(T_h-T_c)/T_h$, and a term dependent on the thermoelectric figure of merit, ZT; η is described by the following equation:

$$(T_h, T_c) = \frac{T_h \quad T_c}{T_h} \frac{\sqrt{1+ZT} \quad 1}{\sqrt{1+ZT} + T_c/T_h}$$

The efficiency of TE devices increases with *ZT*, which is a function of inherent material properties: the Seebeck coefficient, α, the electrical conductivity, σ, the thermal conductivity, k, and the average temperature across the material, T, described in the following equation:

$$ZT = \frac{\alpha^2 \sigma T}{k}$$

In order to maximize *ZT*, a material must have a high Seebeck coefficient and high electrical conductivity, while maintaining a low thermal conductivity, but these parameters are generally interdependent in bulk materials due to opposing dependencies on charge carrier concentration, limiting conventional bulk TE materials to $ZT \sim 1$ (**Figure 1.1**).[9] Consequently, the maximum *ZT* for most materials lies in the carrier concentration range of highly doped semiconductors.

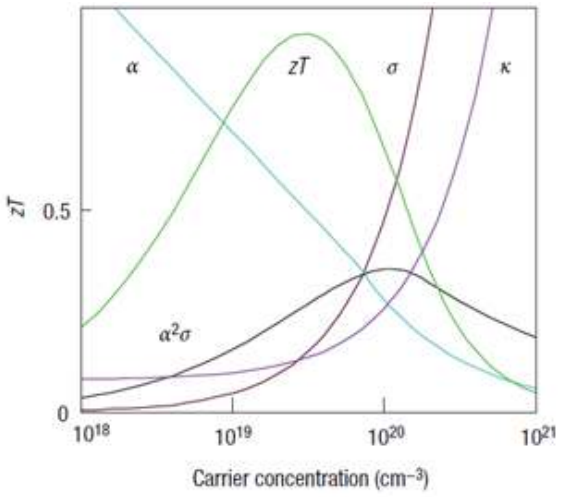

Figure 1.1: A plot showing the interdependence of *ZT*, α, σ, k, and the power factor ($\alpha^2\sigma$) as a function of carrier concentration.[9]

Energy Filtering Approach for Improved Thermoelectric Performance

Various strategies strive to decouple these parameters and improve *ZT* beyond what is possible with doping control.[10–12] Nanocrystalline solids, for example, exhibit improved TE properties over bulk solids due to a depressed *k*, while not affecting electronic properties. Further increases in *ZT* are possible by decoupling α and σ through the incorporation of charge carrier energy filtering nanoscale interfaces, which boost the power factor ($\alpha^2\sigma$) and thus *ZT*.[9,11,13] Energy filtering materials have been demonstrated in heterostructured nanocrystalline materials by conventional solid-state synthetic methods, but control over the phase and distribution of heterostructures, as well as compositional restrictions, limit the insights and application of materials from these approaches.[9,12] As a result, while many theoretical studies have predicted large improvements in thermoelectric performance, a practical understanding of the determinants of energy filtering efficiency and the subsequent effects on *ZT* is limited. Bottom-up assembly of heterostructured TE materials, however, could lead to an experimental platform through which individual TE parameters can be studied and optimized for the rational design of efficient TE materials.

1.2 Bottom-up Assembled Nanocrystal Thin Films

Colloidal nanocrystal solutions can be cast into solid state nanostructured thin films using spin-casting, dip-coating, or drop-casting methods. Generally, this process involves the deposition of NCs onto a solid substrate by evaporating the NC solvent, and the process can be optimized to produce densely packed NC thin films of a desired thickness.[14] Heterogeneous NC thin films can be prepared by mixing different NCs in solution before the film casting steps. By combining precise amounts of different NCs in solution, this strategy affords discrete control over the

nanoscale composition of the resulting material, an advantage that is typically impractical or impossible through traditional solid-state syntheses.

Ge NCs and metal germanide NCs (M-Ge NCs) were chosen as model building blocks for bottom-up assembled, energy filtering TE materials. Like many semiconductors, germanium is a good TE material, and nanostructured Ge-based TE devices exhibit enhanced *ZT* values.[15,16] M-Ge NCs are of particular interest due to the paucity of literature reports of their synthesis, their complex crystal structures, and the ability to tune their work function, and thus their energy filtering properties, by alloying and incorporation of rare earth dopants.[17] By implementing the bottom-up assembly strategy described above, Ge NCs and M-Ge NCs can be precisely combined into a nanostructured thin film, providing a systematically variable experimental platform with which to study fundamental determinants of thermal and electrical transport in these materials (**Figure 1.2**).

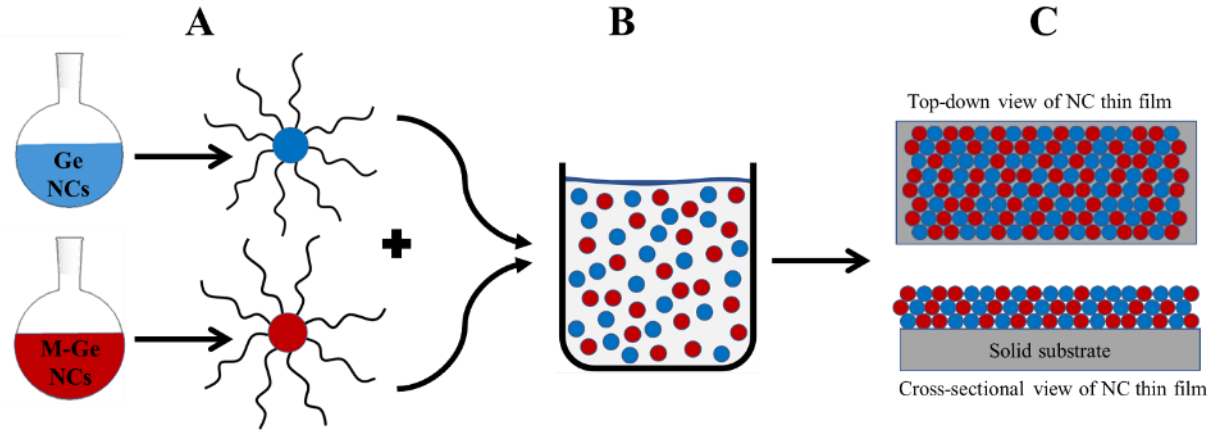

Figure 1.2: Proposed assembly of bottom-up nanocrystal thin-film thermoelectric devices: (A) Colloidal synthesis of Ge NCs and M-Ge NCs, (B) Precise combination of Ge NCs and M-Ge NCs into solution for film casting, (C) Bottom-up assembled Ge/M-Ge NC thin films for systematic study of thermoelectric properties.

1.3 Synthesis of Colloidal Metal Germanide Nanocrystals.

The synthesis of colloidal Ge NCs has developed significantly over the past two decades, and there numerous high-yielding syntheses for Ge NCs which can subsequently be cast into NC thin films.[18–20] However, there are few reports on the synthesis of colloidal M-Ge NCs, so developing syntheses for different M-Ge NCs is required before the energy filtering effects and TE performance of bottom-up assembled Ge/M-Ge NC thin films can be fully examined.[17,21]

Ge NC syntheses typically involve the reduction of a Ge precursor to produce colloidal nanoscale products via a controlled nucleation and growth process. A one-pot synthesis developed by Xue and coworkers accomplishes the reductive thermolysis of Ge(II) halide precursors in oleylamine ($C_{18}H_{35}NH_2$), which serves as the solvent, reductant, and surface capping ligand.[22] This synthesis is favorable for its simplicity, lack of highly reactive reagents, and its consistent high-yield production of crystalline colloidal GeNCs.

FeGe NCs were synthesized by introducing a $Fe(CO)_5$ precursor into a solution of growing Ge NCs in a similar high temperature solution reduction reaction.[17] Based on this result, it was hypothesized that other M-Ge NCs could be similarly synthesized by introducing a metal(0) complex during the nucleation and growth of the Ge particles. The results presented in Chapter 2 detail an in-depth exploration of the synthesis of colloidal NiGe NCs, and preliminary results of colloidal FeGe NC and PdGe NC preparations are also discussed.

1.4 Surface Modification of Germanium Nanocrystals and Film Casting

The colloidal nature of Ge and M-Ge NCs is critical to the bottom-up assembly of NC thin films. The Ge NCs and M-Ge NCs are colloidal because the particle surfaces are capped by long aliphatic oleylamine molecules (OAm). The OAm molecules stabilize the NCs in nonpolar solvents so that the NCs can be combined and cast into thin films. However, OAm is not

electrically conductive and prevents tight packing of the conductive inorganic NC cores in the thin films, so the OAm ligands must be removed before TE performance can be examined (**Figure 1.3**).

There are reports on the removal of OAm ligands from Ge NC surfaces, but attempts to replicate these results were generally unsuccessful. Using a combination of methods from the literature, a high-temperature sulfur treatment[18,23] of Ge NCs was explored and developed, which is described in Chapter 3. Using this method, OAm ligands were removed from the Ge NC surface and replaced with hydrazine (N_2H_4). Thin films cast from hydrazine-capped Ge NCs were found to be much more electrically conductive than films cast from OAm-capped Ge NCs, though further development of the film casting techniques is required for full exploration of the TE performance of bottom-up assembled Ge/M-Ge NC thin films.

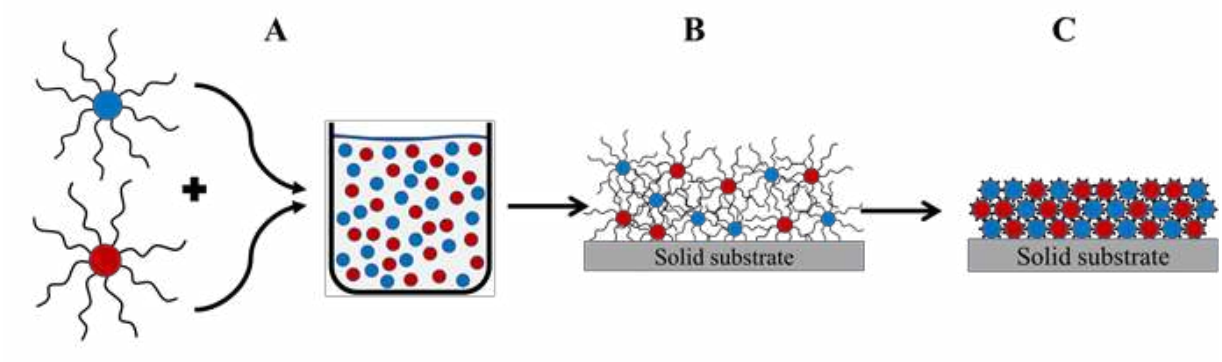

Figure 1.3: Proposed scheme for the bottom-up assembly of heterostructured NC thin films: (A) Colloidal synthesis of Ge NCs and M-Ge NCs and precise combination of Ge NCs and M-Ge NCs into solution for film casting, (B) Initial deposition of the Ge NCs and M-Ge NCs results in NC thin film with long aliphatic surface ligands increasing interparticle distance and poor electrical conductivity, (C) Removal of long, aliphatic surface ligands for shorter ligands that decrease inter-particle distance and improve electrical conductivity.

Chapter 2: Colloidal Synthesis of Nickel Germanide Nanocrystals

Introduction

Germanium and Ge-based nanomaterials possess ideal physical transport properties for various applications in solid-state devices, such as thermoelectric materials and photovoltaics.[1] Colloidal preparations of Ge-based nanomaterials are particularly desired because solution-phase processing and bottom-up assembly of nanostructured devices is more affordable and permits more control over nanoscale composition, but the synthesis of colloidal Ge-based nanomaterials is challenging, which has impeded the investigation and characterization of their physical properties.[1,24] Metal-germanide nanomaterials are of particular interest for use as thin-film ohmic contacts in microfabricated devices, and he development of metal germanide nanomaterials could play an essential role in the growing use of germanium-based electronic devices that possess superior performance over silicon-based devices.[25–29]

Germanium Nanocrystal Synthesis

Ge NC syntheses have improved significantly over the past two decades, and crystalline colloidal Ge NC products are achievable through several routes.[1] These syntheses typically involve reduction of organogermane or germanium salt precursors in a high boiling point solvent to initiate a controlled nucleation and growth process.[22,24,30,31] Because Ge is highly covalent, high temperatures are required for precursor reduction and particle crystallization, which necessitates the use of high boiling point solvents.[32] However, the use of strong reducing agents is not conducive to the synthesis of consistent and high-yielding products.[33]

Alternatively, a one-pot synthesis developed by Xue and coworkers produces crystalline colloidal Ge NCs through the reductive thermolysis of Ge(II) halide precursors in oleylamine (OAm), which serves as the solvent, reductant, and particle surface capping ligand.[22] This

synthesis is favorable for its simplicity, lack of highly reactive reagents, and its consistently high-yield production of crystalline colloidal GeNCs.

Ge-based Nanomaterial Synthesis

Many of the various Ge NC synthetic approaches have been adapted to synthesize colloidal Ge-based nanomaterials, such as GeSn, GeTe, GeSe, GeS, and Ge/Cds and GeSn/CdS core/shell nanocrystals, many of which are useful for applications in photovoltaics and field-effect transistors, among others.[23,34–40] However, there is a paucity of metal germanide NC syntheses. A FeGe NC synthesis was reported by Schaak and coworkers, while Prieto and coworkers reported the synthesis of Fe_2GeS_4 NCs.[17,21] The recent advances in the synthesis of colloidal Ge-based nanocrystals has been rapid, but this area still lags behind the vast methods for metal and other elemental and compound semiconductor nanocrystal materials. These previous works have laid the groundwork for future explorations, but further synthetic development is necessary and depends upon more generalizable approaches to the synthesis of Ge-based materials.

Building upon recent developments in Ge nanomaterial synthesis, the results in this Chapter describe the synthesis of NiGe nanocrystals via injection of a nickel(0) precursor into a solution of Ge(II) halide and high-boiling point solvent. This method produces colloidal $Ni_{19}Ge_{12}$ NCs, which is unexpected based on the instability of this phase at room temperature. Furthermore, the synthetic mechanism was investigated, showing that neither the molar ratio of Ni:Ge reactants nor the injection temperature of the Ni(0) precursor affect the crystal phase of the resulting product. However, the addition of a trioctylphosphine cosolvent produces Ni_1Ge_1 NC products. Finally, the synthesis is extended to produce PdGe and FeGe NCs.

Experimental

Synthesis of Germanium Nanocrystals. In a glovebox, 139 mg (0.6 mmols) of $GeBr_2$ and 5 mL of oleylamine (OAm) were added to a three-neck round bottom flask, equipped with a glass-coated stirbar and condenser. The apparatus was transferred out of the glovebox and placed under positive N_2 pressure. The reaction was heated to a temperature of 260 °C, at 5 °C/min, followed by a 1 hr soak at 260 °C. After cooling, the brown product was precipitated by centrifugation at 10000 xg with a mixture of toluene, ethanol, and acetone. After this was repeated twice, the particles were resuspended in toluene, and stored in a nitrogen glovebox.

Synthesis of Nickel Germanide Nanocrystals. In a glovebox, 139 mg (0.6 mmols) of $GeBr_2$ and 5 mL of OAm were added to a three-neck round bottom flask, equipped with a glass-coated stirbar and condenser. The apparatus was transferred out of the glovebox and placed under positive N_2 pressure. The reaction was heated to a temperature of 310 °C, at 5 °C/min. When the solution reached the target temperature, 8 mL of a bis(1,5-cyclooctadiene)nickel(0) in toluene was slowly injected, immediately turning the solution black. In the standard synthesis, $Ni(COD)_2$ was injected at 260 °C and the amount of $Ni(COD)_2$ was varied between 0.006 mmol and 0.9 mmol. When injection temperature was varied between 180 °C and 300 °C, 0.4 mmol $Ni(COD)_2$ was used injected. A needle was inserted into one of the side necks of the flask to vent away the volatile toluene so that the solution could continue heating to 310 °C, where it remained for 1 hr. After cooling, the black product was precipitated by centrifugation at 10000 xg with a mixture of toluene, ethanol, and acetone. After this was repeated twice, the particles were resuspended in dry toluene, and stored in a nitrogen glovebox.

Ge NC, TOP-cosolvent Synthesis, 60% TOP. In a glovebox, 139 mg (0.6 mmols) of $GeBr_2$, 2 mL of OAm and 3 mL of TOP were added to a three-neck round bottom flask, equipped

with a glass-coated stirbar and condenser. The apparatus was transferred out of the glovebox and placed under positive N_2 pressure. The reaction was heated to a temperature of 320 °C, at 5 °C/min, where it remained for 1 hr. After cooling, the brown product was precipitated by centrifugation at 10000 xg with a mixture of toluene, ethanol, and acetone. After this was repeated twice, the particles were resuspended in toluene, and stored in a nitrogen glovebox.

40:60 NiGe, TOP-cosolvent Synthesis. In a glovebox, 139 mg (0.6 mmols) of $GeBr_2$, and a 5 mL mixture of OAm and TOP was added to a three-neck round bottom flask, equipped with a glass-coated stirbar and condenser. The % vol. of TOP in the reaction was varied between 1% and 60% for each experiment. The apparatus was transferred out of the glovebox and placed under positive N_2 pressure. The reaction was heated to a temperature of 320 °C, at 5 °C/min. After the solution turned brown, 8 mL of a 0.5 M solution of $Ni(COD)_2$ in toluene (0.4 mmol Ni total) was slowly injected, immediately turning the solution black. A needle was inserted into one of the side necks of the flask to vent away the volatile toluene so that the solution could continue heating to 320 °C, where it remained for 1 hr. After cooling, the black product was precipitated by centrifugation at 10000 xg with a mixture of toluene, ethanol, and acetone. After this was repeated twice, the particles were resuspended in toluene, and stored in a nitrogen glovebox. To anneal the products, an aliquot of the sample was dried onto a glass coverslip and heated to the desired temperature in a tube furnace under nitrogen flow.

Synthesis of FeGe NCs. Reactions were prepared in a nitrogen glovebox identically to the setup for the NiGe NC synthesis detailed above. As the reaction was heated to 310 °C, 0.079 mL of iron pentacarbonyl was injected at 260 °C. The products were isolated using the same procedures for NiGe NC synthesis, and stored in a nitrogen glovebox

Synthesis of PdGe NCs. Reactions were prepared in a nitrogen glovebox identically to the setup for the NiGe NC synthesis detailed above. As the reaction was heated to 310 °C, 0.346 g (0.3 mmol) tetrakis(triphenylphosphine)palldium(0) dissolved in 5 mL toluene was injected at 260 °C. The products were isolated using the same procedures for NiGe NC synthesis and stored in a nitrogen glovebox.

Characterization. The products of each synthesis were prepared for X-Ray diffraction (XRD) analysis by drying an aliquot of the colloidal toluene solution onto a silicon XRD sample holder. Rigaku Smartlab and Rigaku Ultima instruments were used for XRD. Transmission electron microscopy (TEM) images and large area compositional data from energy dispersive X-ray spectroscopy (EDS) were collected on a Philips CM-20 TEM, while high-resolution TEM images and single particle EDS scans were collected with a JEOL 2800 TEM instrument.

Results and Discussion

Synthesis Germanium Nanocrystals. Colloidal germanium nanocrystals (Ge NCs) were synthesized by heating $GeBr_2$ to 310 °C in a oleylamine (OAm). In this reaction, the $Ge(II)Br_2$ precursor is reduced by the OAm solvent and begins to nucleate Ge particles around 220° C, indicated by the dark brown color that forms around this temperature (**Figure 2.1**). The reaction is then heated to 310 °C to complete the growth of the particles and induce Ge crystallization. TEM imaging showed that the Ge NCs were quasi-spherical in shape and were 8.2 ± 1.3 nm in diameter (**Figure 2.2**). XRD analysis confirmed the crystallinity of the particles, showing the reflections of a cubic Ge phase, with peak broadening characteristic of nanoscale phases (**Figure 2.3**).

Figure 2.1 Color progression of the standard $GeBr_2$-OAm reaction with evidence of Ge particle formation and growth at 230°C-240°C.

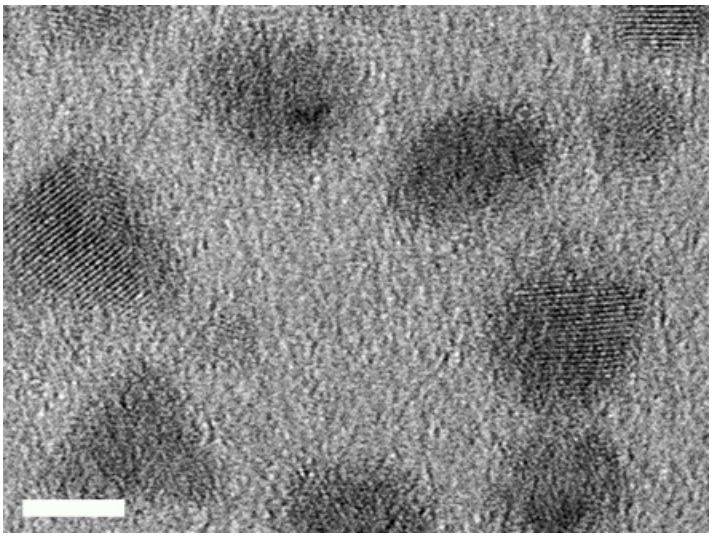

Figure 2.2:. TEM image of GeNCs from standard $GeBr_2$-OAm synthesis. (Scale bar = 5 nm)

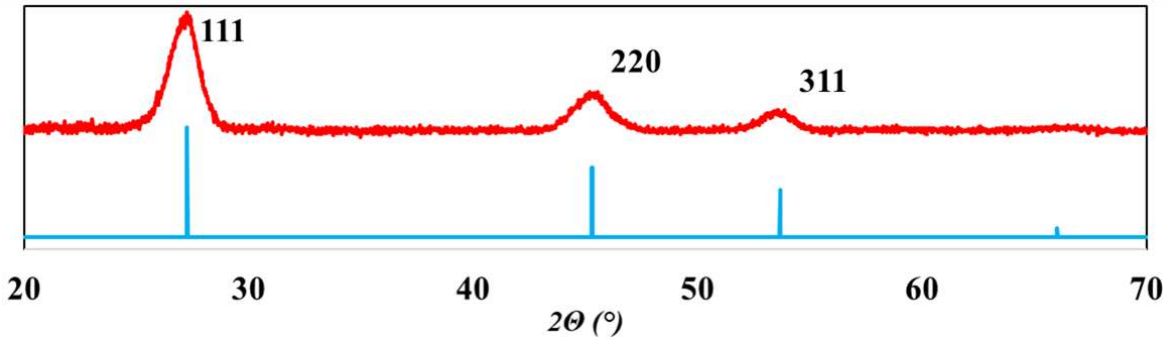

Figure 2.3: XRD patterns of (A) GeNCs synthesized from standard OAm-$GeBr_2$ reaction, and B) predicted Ge crystal.

Synthesis of $Ni_{19}Ge_{12}$ Nanocrystals. Nickel germanide nanocrystals (NiGe NCs) were synthesized by introducing a nickel (0) precursor into a hot solution of growing germanium particles. TEM images showed that the particles were quasi-spherical with a diameter of 8.9 ± 2.1

nm, similar to the size and shape of the Ge-only NC products (**Figure 2.4**). Despite varying the Ni:Ge precursor ratio, XRD patterns indicate that the products consistently formed the $Ni_{19}Ge_{12}$ crystal phase at Ni:Ge between 20:80 and 50:50 (**Figure 2.5**). Stable colloidal products were isolated from lower Ni:Ge ratios, but XRD analysis indicates the presence of Ge phase only in this range of reactant ratios. Ni:Ge above 50:50 resulted in no or minimally stable colloidal products. *In situ* energy dispersive X-ray spectroscopy (EDS) analysis of NiGe NCs showed Ni:Ge ratios consistent with $Ni_{19}Ge_{12}$ stoichiometry (**Table 2.1**) for Ni:Ge between 20:80 and 50:50, and single particle EDS line scans showed that the Ni and Ge are uniformly distributed within each particle (**Figure 2.6**). The consistent formation of the $Ni_{19}Ge_{12}$ phase was unexpected because the $Ni_{19}Ge_{12}$ phase is only stable at temperatures above 400 °C in bulk and at Ni:Ge ratios above 50% Ni (**Figure 2.7**). The temperature of the solution reaction never exceeded 310° C, and the ratio of Ni:Ge precursors in reactions that resulted in stable colloidal products were at or below 50:50, so the NC phase was expected to adopt a mixture of Ni_1Ge_1 and pure Ge. At 60% Ni, closer to the stoichiometry of $Ni_{19}Ge_{12}$, no colloidal product was isolated. Due to the large energetic contribution of surface energy in nanoscale materials, these can adopt crystal phases not otherwise stable in the analogous bulk material.[41]

Another unexpected result of the $Ni_{19}Ge_{12}$ phase formation is the exclusion of Ge from the isolated NC product. In the bulk, $Ni_{19}Ge_{12}$ forms at Ni-rich at %, but from the Ge-rich reactant ratios that result in NC products, there must be excess Ge that is not apparent in the XRD patterns, suggesting an amorphous phase. TEM images (**Figure 2.4**), however, show no indication of an amorphous phase, and the large area and line-scan (**Figure 2.6**) EDS data also indicate Ni:Ge at % ratios consistent with the presence of the $Ni_{19}Ge_{12}$ phase only. Instead, it is possible that the excess Ge remains in solution as a stable molecular product, for example as $Ge(OAm)_2$, or that it

precipitates as a non-colloidally stable elemental solid product. For reactions with Ni:Ge precursor ratios of 1:99-10:90, XRD patterns indicate that crystalline Ge only phase NCs were formed, although Ni was still detected in EDS spectra at the reactant ratios, suggesting the presence of disordered Ni in the isolated colloidal product. For a Ni:Ge ratio of 10:90, XRD suggested that the products were poorly crystalline, and EDS also indicated Ni incorporation at levels consistent with the reactant stoichiometry, but the formation of a fully crystalline Ge or NiGe phase is somehow limited.

Table 2.1: Composition of the products of NiGe NC syntheses using various Ni:Ge ratios as determined by large area EDS.

Ni:Ge precursor ratio	% Ni in product	% Ge in product
1:99	3.5 ± 1.5	96.5 ± 1.5
5:95	3.6 ± 1.3	96.4 ± 1.4
10:90	10.1 ± 1.2	89.9 ± 1.2
20:80	62.1 ± 1.4	37.9 ± 1.4
30:70	64.2 ± 2.2	37.3 ± 2.2
40:60	64.2 ± 2.6	35.8 ± 2.6
50:50	63.6 ± 2.1	36.4 ± 2.1

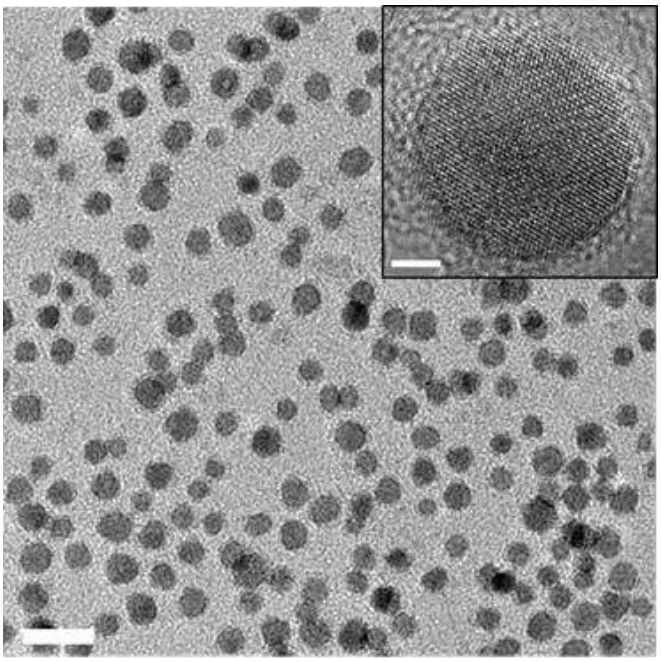

Figure 2.4: TEM image of the spherical $Ni_{19}Ge_{12}$ nanocrystals synthesized by injecting 0.4 mmol $Ni(COD)_2$ into a hot OAm solution of growing Ge particles. The inset shows a High-Resolution TEM (HRTEM) image of a particle and its lattice fringes.

(Scale bar = 20 nm; 2 nm for inset)

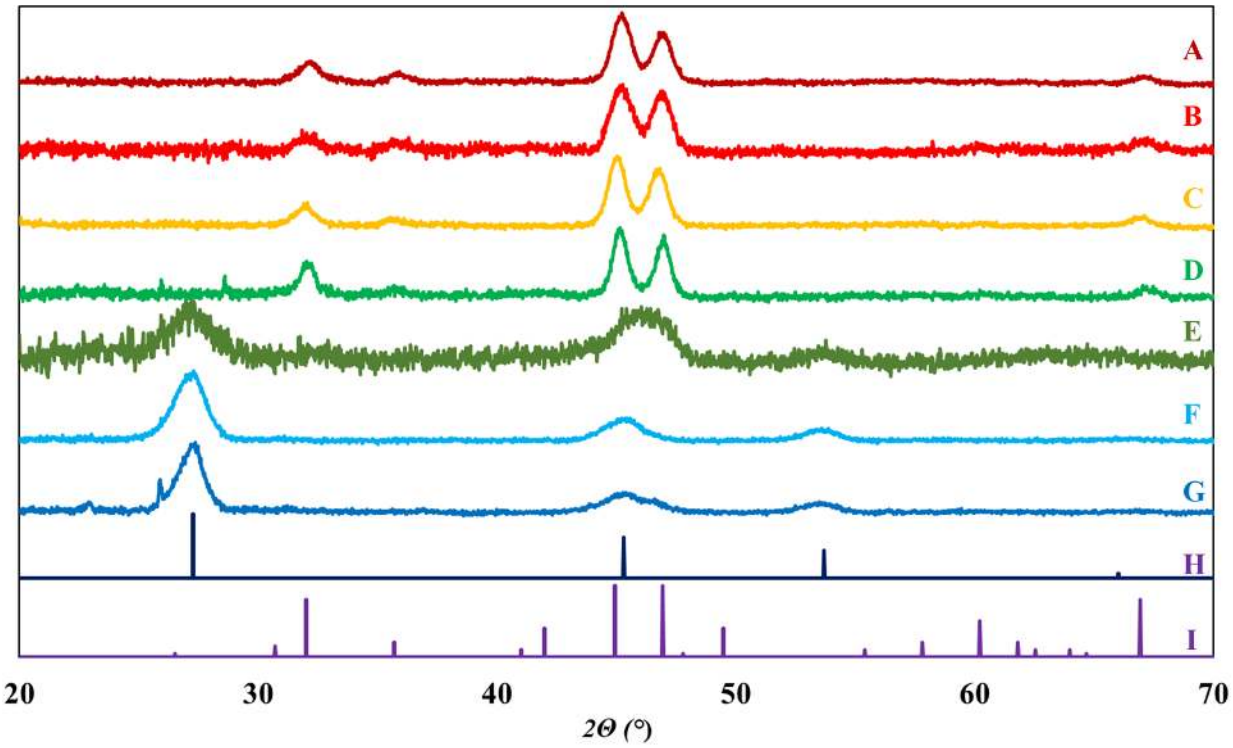

Figure 2.5: XRD patterns of (I) predicted $Ni_{19}Ge_{12}$ phase, (H) predicted Ge phase, and of the products from reactions containing varying ratios of Ni:Ge reactants: (G) 1:99, (F) 5:95, (E) 10:90, (D) 20:80, (C) 30:70, (B) 40:60, (A) 50:50.

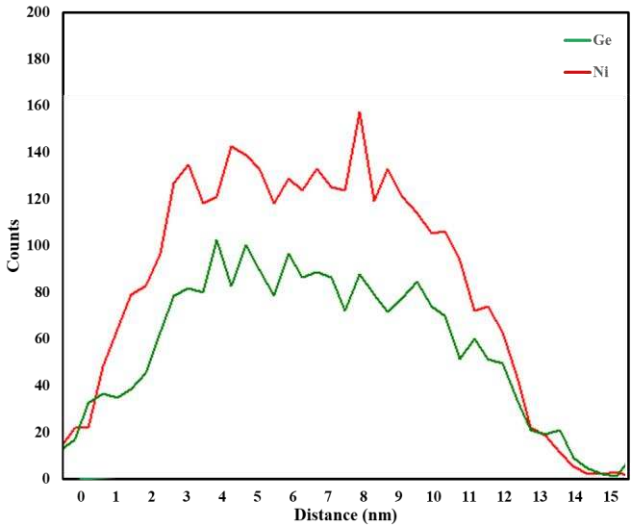

Figure 2.6: Single particle EDS line scan of $Ni_{19}Ge_{12}$ NC showing uniform distribution of Ni (red) and Ge (green) across a single NC.

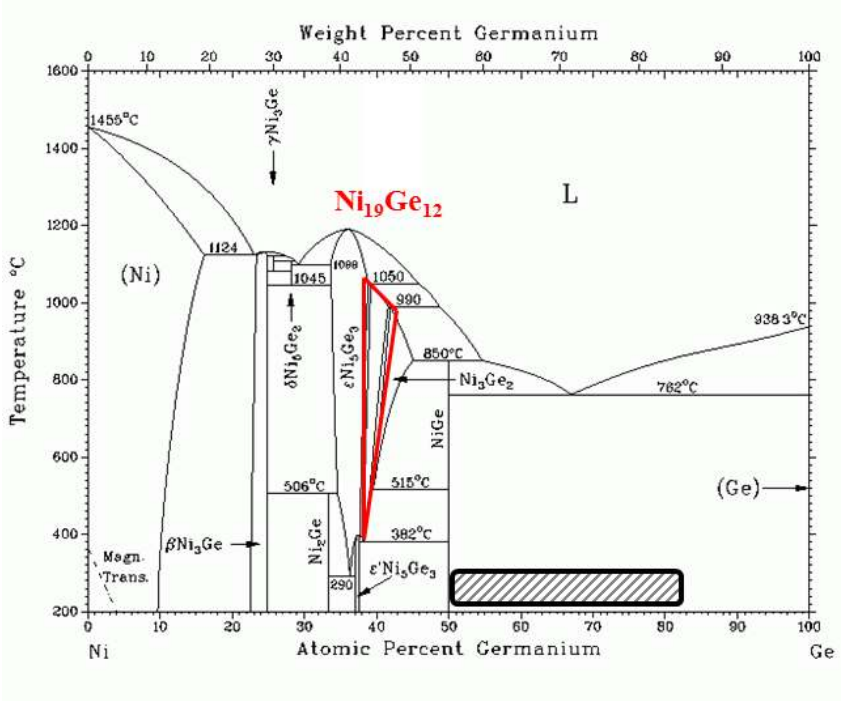

Figure 2.7: Ni-Ge phase diagram, with the $Ni_{19}Ge_{12}$ phase outlined in red. The range of the Ni:Ge molar ratio and temperature of the synthesis (shaded area) suggested that the products should have produced a Ni_1Ge_1 phase.

Next, the importance of the order of nucleation of Ge and Ni particles on the formation of NiGe phases was explored. The formation of Ge particles begins around 200 °C as indicated by the color change of the reaction from orange to brown. $Ni(COD)_2$ was injected into the reaction at different temperatures above and below this temperature. When Ni is injected at 180°C, well below the nucleation temperature for Ge particles, only a black solid precipitate is recovered. XRD results show that at 200°C or above, the temperature at which Ni is injected does not affect the phase of the isolated product (**Figure 2.8**). However, This result suggests that when there are few or no Ge nuclei in the reaction solution at the time of the Ni(0) injection, then the Ni(0) will not precipitate onto Ge particles, and instead, aggregate out of solution.

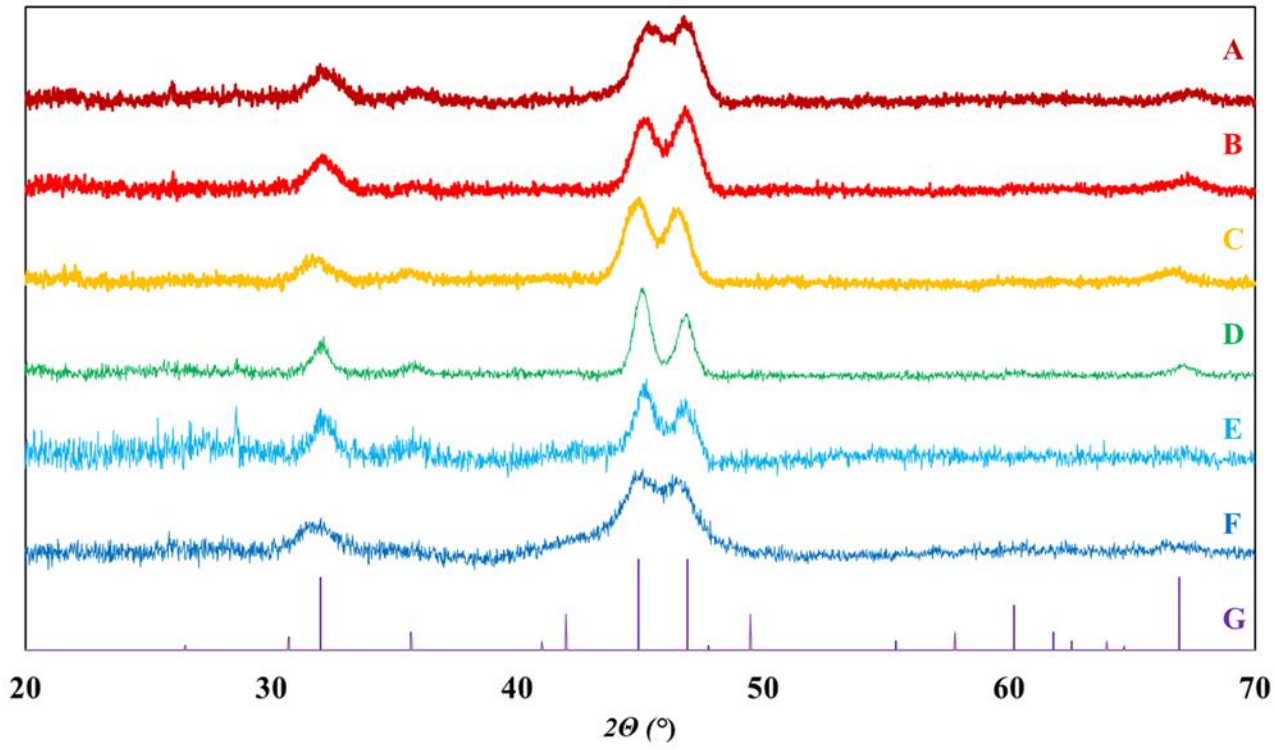

Figure 2.8: XRD patterns of (G) Predicted $Ni_{19}Ge_{12}$ phase, and 40:60 Ni:Ge reactions with $Ni(COD)_2$ injected at various temperatures: (F) 200°C, (E) 220°C, (D) 240°C, (C) 260°C, (B) 280°C, (A) 300°C.

Finally, the crystallinity of the Ge particles at the injection point was investigated. The reaction was held at 260° C for various amounts of time before the Ni(0) was introduced, allowing the Ge particles to crystallize before the Ni(0) injection.[42] XRD revealed that injection of Ni(0) after more than 30 min at 260°C produces poorly crystalline products (**Figure 2.9**). EDS spectra indicate limited Ni content (~15%) in the product, suggesting that Ni adsorbed and diffused into the Ge particles, but that the formation of either Ge or NiGe phases was inhibited, further suggesting that Ni(0) must be incorporated during the initial stages of Ge particle formation (**Table 2.2**). It is interesting to note that although the increased crystallization of Ge limited the amount

of Ni incorporated into the NCs, and that the Ni injected at longer soak times also disrupted the crystalline state of the resulting NCs.

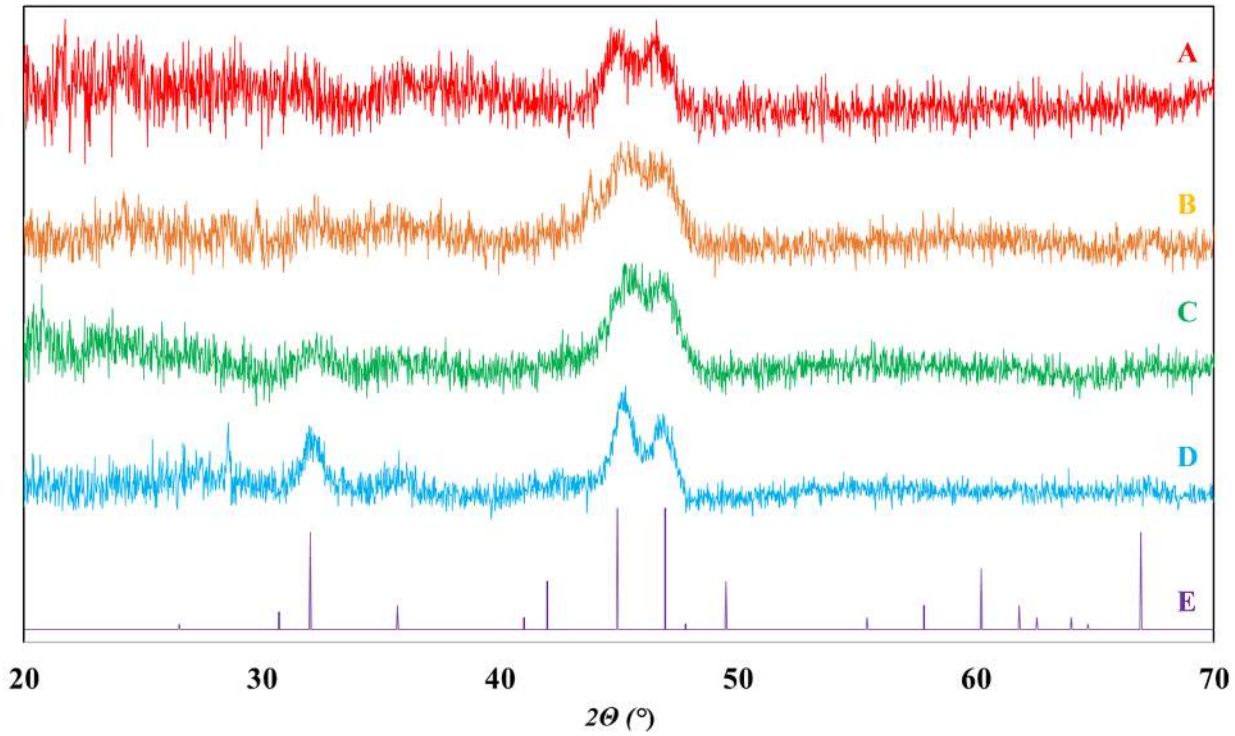

Figure 2.9: XRD patterns of (E) Predicted $Ni_{19}Ge_{12}$ phase, and 40:60 Ni:Ge reactions with a $Ni(COD)_2$ injection at 260°C delayed by (D) 15 min, (C) 30 min, (B) 1 hr, (A) 2 hr.

Table 2.2: Composition of the products of 40:60 Ni:Ge reactions with a delayed $Ni(COD)_2$ injection, as determined by large area EDS scans. The reactions were held at 260 °C for various amounts of time before injection of Ni(0) precursor to allow growth and crystallization of Ge particles.

Time at 260 °C Before $Ni(COD)_2$ Injection	% Ni in product	% Ge in product
0 min	64.2 ± 2.6	35.8 ± 2.6
15 min	62.1 ± 4.3	37.9 ± 2.7
30 min	15.3 ± 5.9	84.7 ± 6.5
1 hr	13.2 ± 6.8	86.8 ± 5.9
2 hr	12.8 ± 9.2	87.2 ± 7.6

Trioctylphosphine-cosolvent Synthesis. Based on the findings of previous work,[18] and given the apparently strong effect of NC surface energy on crystal phase, we hypothesized that the weaker interaction between the trioctylphosphine (TOP) solvent and the Ge particle surface as compared to Ge-OAm would affect the phase of the NiGe NC product. In agreement with this hypothesis, it was found that when the concentration of TOP was 40-60 vol % in OAm, the nucleation temperature, size, and shape of Ge-only NCs were affected. The temperature at which the solution turned brown, an indication of particle nucleation, increased with increasing TOP concentration, meaning that reduction of $GeBr_2$ required higher temperatures. This increase in nucleation temperature may be due to the proportional decrease in OAm concentration with increasing TOP concentration. TOP is not reducing, whereas at high temperatures OAm is. In spite of the delayed particle growth, the reactions still produced colloidal Ge NCs, and TEM imaging showed that the particles were much larger and exhibited distinct faceting in the shape of prismatic rods and decahedra (**Figure 2.10**).

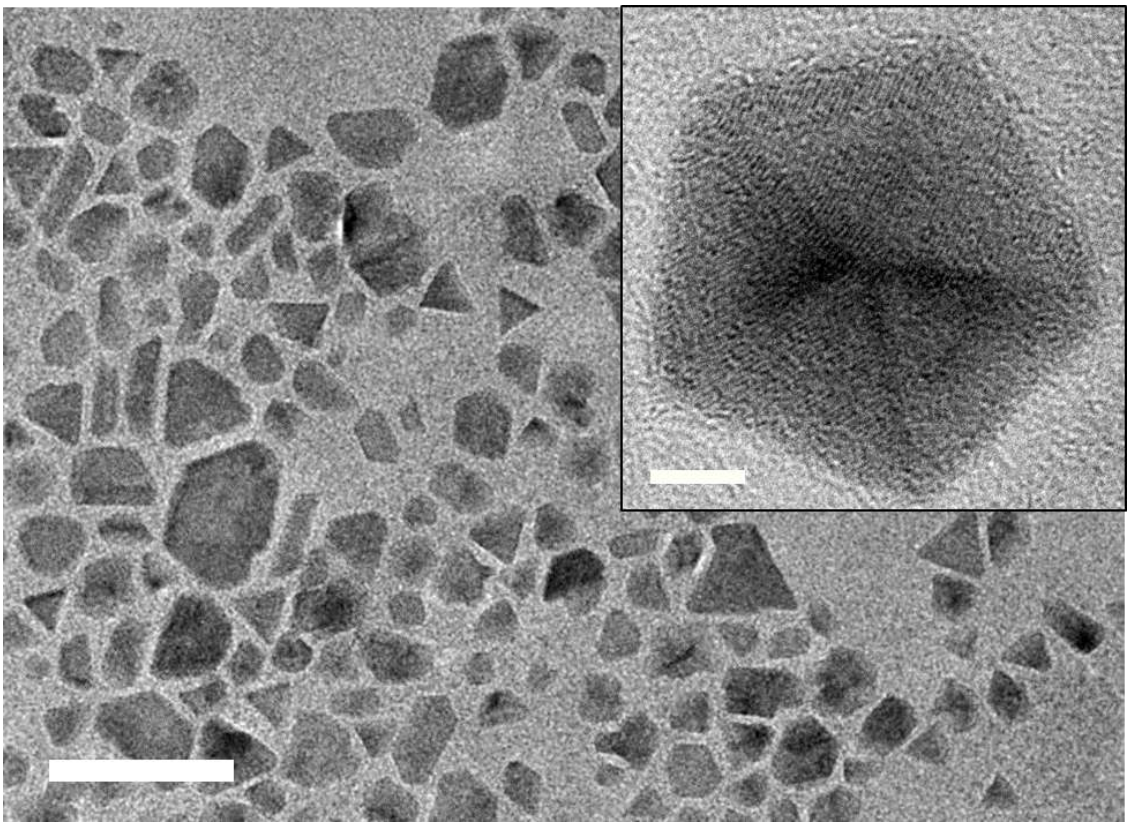

Figure 2.10: TEM image of larger, faceted Ge NCs produced from $GeBr_2$ synthesis using 60% by vol. TOP cosolvent in OAm (scale bar = 50 nm). Inset: Hi-resolution image of polyhedral Ge NC from same sample (Scale bar = 5 nm).

Extending this TOP co-solvent method to the NiGe NC synthesis, it was found that at when the solvent was 20-50% TOP by volume, the isolated products adopted the Ni_1Ge_1 phase, in contrast to the $Ni_{19}Ge_{12}$ phase that formed under nearly all other reaction conditions (**Figure 2.11**). However, EDS quantification of the product composition revealed that the Ni:Ge ratio of the TOP cosolvent products matched the Ni:Ge ratios from OAm-only reactions, which were around 63:37 Ni:Ge, matching the ratio for a $Ni_{19}Ge_{12}$ crystal phase, not the 50:50 ratio expected for the Ni_1Ge_1 phase. Initially, it was suspected that the extra Ni from EDS scans was due to unreacted Ni precursor or amorphous Ni that was not removed

during the workup, but EDS line scans of individual particles revealed that the Ni:Ge distribution in the individual particles was approximately 2:1 Ni:Ge (**Figure 2.12**).

When the sample was dried onto a glass slide and annealed at 300 °C, the products reverted to the $Ni_{19}Ge_{12}$ phase, matching the ratio observed in the EDS analysis. During the reaction there is a large excess of OAm and TOP in solution, but during the annealing step, almost all the OAm and TOP has been removed. Evidently, the presence of TOP during the reaction somehow forces the formation of the Ni_1Ge_1 phase even though the Ni:Ge ratio does not match this phase. It is unclear how the presence of TOP drives this change, and further experiments using other cosolvents would be necessary to form any definitive conclusions, but crystal phase formation mediated by surface ligands has been documented in other NC systems.[43]

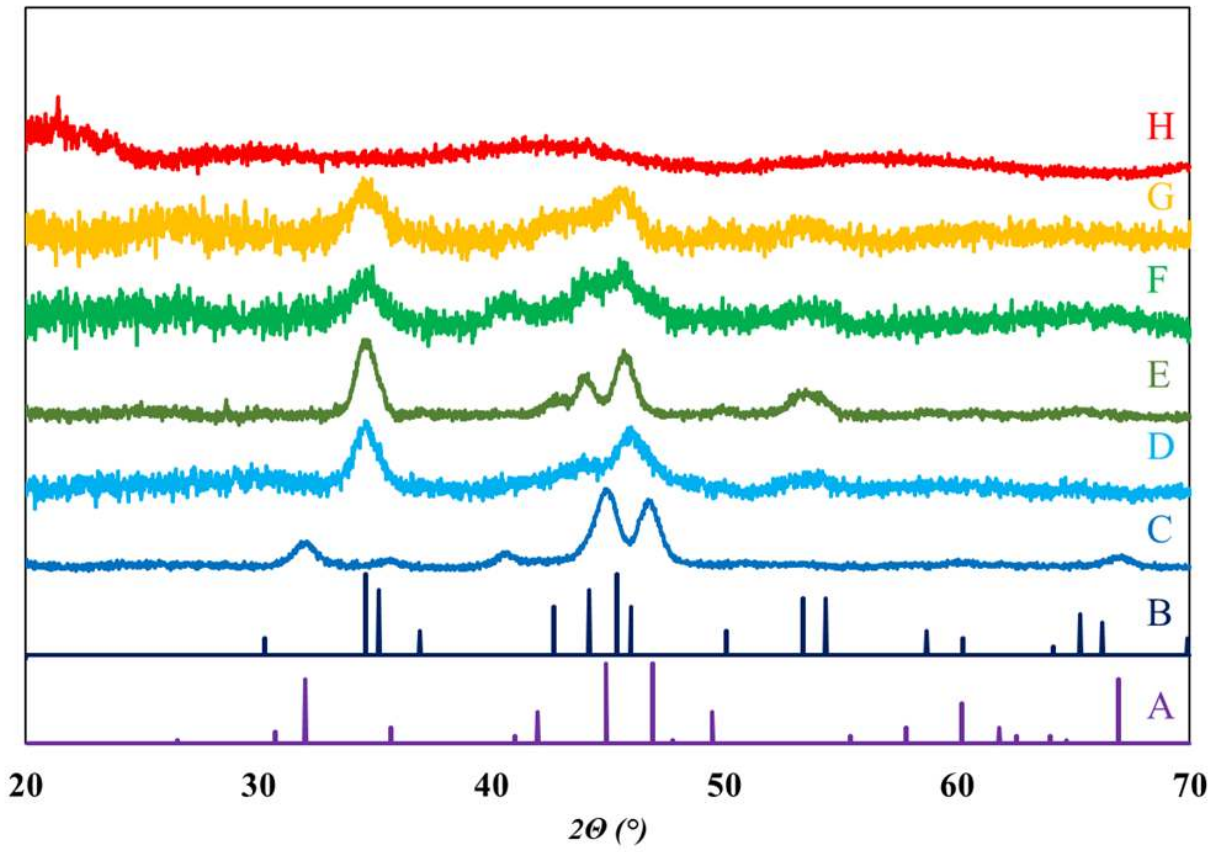

Figure 2.11: XRD patterns of (A) predicted $Ni_{19}Ge_{12}$, (B) predicted Ni_1Ge_1, and the products from NiGeNC reactions using (C) 5% TOP, (D) 20% TOP, (E) 30% TOP, (F) 40% TOP, (G) 50% TOP, (H) 60% TOP by volume.

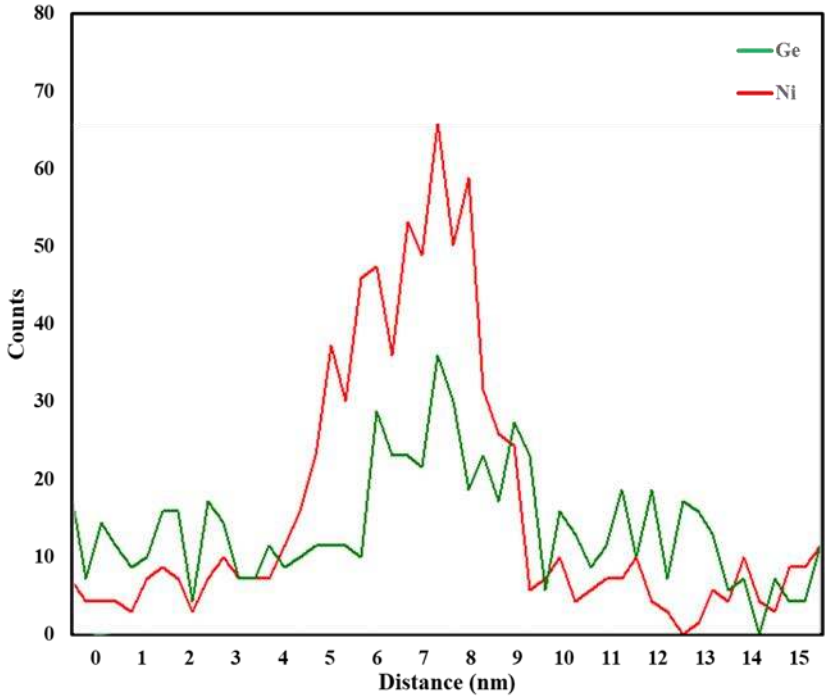

Figure 2.12: Single particle EDS line scan of Ni_1Ge_1 NC from a 35% TOP cosolvent reaction. The Ni (red) and Ge (green) are uniformly distributed across the individual particle, similar to the elemental distribution from the $Ni_{19}Ge_{12}$ NCs from OAm-only syntheses.

Colloidal Synthesis of PdGe and FeGe NCs. The synthesis of NiGe NCs was accomplished by injecting a Ni(0) precursor into a solution of growing Ge particles, and it was hypothesized that injection of other metal(0) precursors would produce other metal germanide NCs. Iron(0) pentacarbonyl was injected, in a 50:50 Fe:Ge precursor ratio, to produce FeGe NCs, and TEM of the product showed that individual NCs were synthesized and were of a similar size and shape to the NiGe NCs (**Figure 2.13**). XRD analysis revealed that the colloidal product was Fe_1Ge_1 NCs, indicating that the synthesis was successful (**Figures 2.14**). Similarly, colloidal PdGe nanoparticles were synthesized, and TEM images showed individual particles around 10 nm in diameter (**Figure 2.15**). Unlike the NiGe NC and FeGe NC syntheses however, XRD analysis of

the PdGe colloidal products revealed that the material was amorphous, but after annealing the sample at 400 °C, the products adopted a Pd_2Ge phase (**Figure 2.16**).

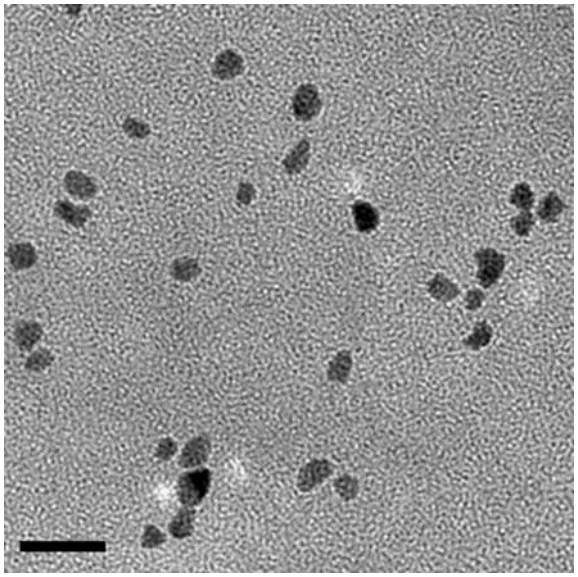

Figure 2.13: TEM image of colloidal Fe_1Ge_1 NCs (Scale bar = 50 nm).

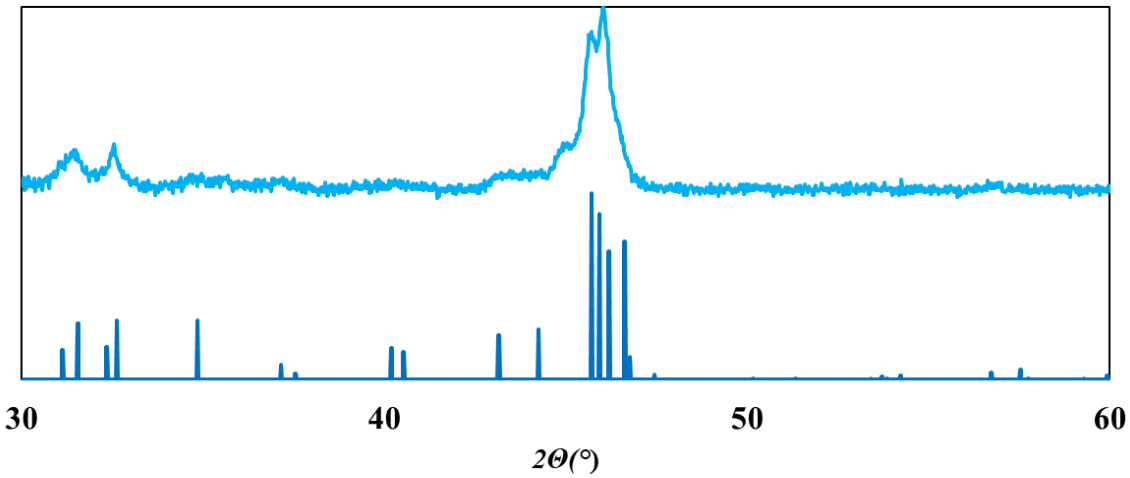

Figure 2.14: XRD patterns of FeGe NCs (top) and predicted Fe_1Ge_1 pattern (bottom).

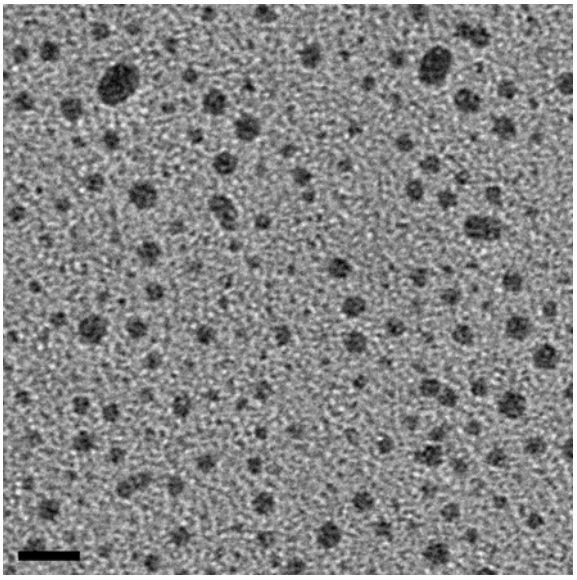

Figure 2.15: TEM image of colloidal PdGe nanoparticles (Scale bar = 10 nm).

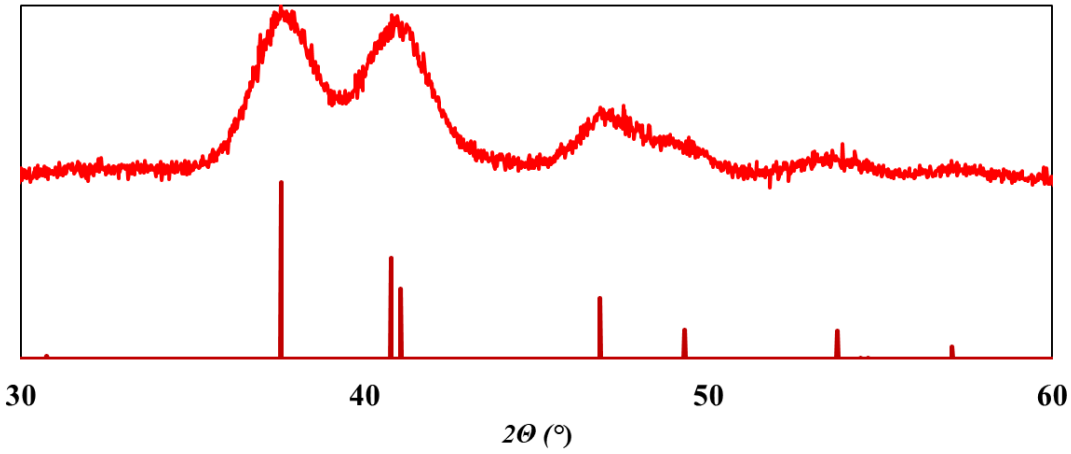

Figure 2.16: XRD patterns of annealed PdGe nanoparticles (top), matching the predicted Pd_2Ge pattern (bottom).

Conclusions and Future Work

The synthesis of NiGe NCs was explored thoroughly and determined to favor the formation of a $Ni_{19}Ge_{12}$ phase that was unexpected based on the temperature and Ni:Ge ratio. The insights from the mechanistic studies led to the development of a proposed mechanism, which could be

extended to other metal-Ge nanomaterial syntheses (**Figure 2.17**). It is proposed that Ge particles provide a nucleation point onto which injected Ni(0) atoms can precipitate to form NiGe particles, which crystallize after a high temperature soak. For molar ratios between 20:80 and 50:50 Ni:Ge and Ni(0) injections between 200°C and 300°C, the product will form the $Ni_{19}Ge_{12}$ phase with a uniform distribution of Ni and Ge in the individual particles. Injections well before the formation of Ge particles or after Ge particle crystallization lead to amorphous or colloidally unstable products.

Based on the proposed mechanism, it was hypothesized that other M-Ge NCs could be similarly produced by injecting other metal(0) precursors, and the successful preparation of Fe_1Ge_1 NCs supported this hypothesis. Although the PdGe synthesis produced amorphous colloidal material, the product crystallized after annealing, confirming that Pd and Ge were incorporated into the same particles, which also supports the proposed mechanism. Future experiments should continue to test the proposed mechanism via injection of other metal(0) precursors, which may enable the synthesis of many other M-Ge NCs.

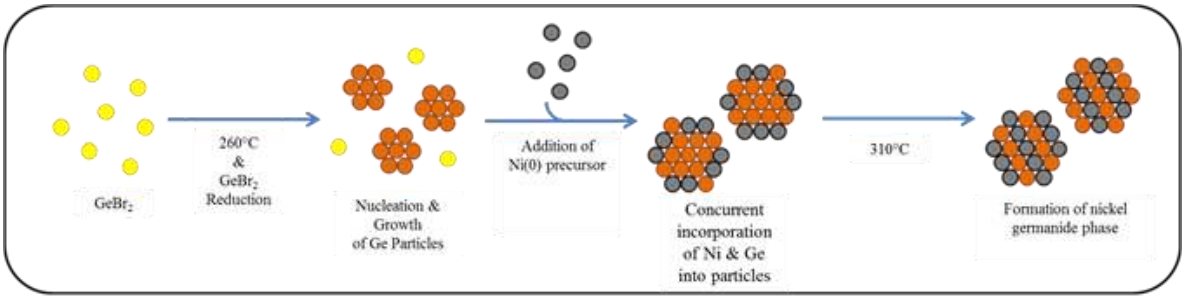

Figure 2.17: Proposed mechanism for the synthesis of NiGe NCs.

The use of a TOP cosolvent was determined to alter Ge NC shape and stabilize the formation of the Ni_1Ge_1 phase, but it is unclear how the TOP cosolvent causes these effects. TOP has a tertiary phosphine headgroup compared to the primary amine headgroup of OAm, which

explains why the addition of TOP cosolvent required higher temperatures to initiate Ge particle growth. It is possible that the altered particle growth temperature is the underlying cause for the observed differences. Additionally, because TOP is sterically bulkier than OAm, it is reasonable to expect that lattice strain could be induced by surface-coordinated TOP ligands. When the Ni_1Ge_1 NCs were annealed outside of solution, the TOP would no longer exert any lattice strain, allowing the formation of the $Ni_{19}Ge_{12}$ crystal phase that matches the Ni:Ge ratio. Based on the present data, however, no definitive conclusion can be made. Further experiments using cosolvents of differing sterics and other ligand headgroups could resolve the underlying mechanisms behind this effect, and potentially allow the formation of other crystal phases or designed particle morphologies.

Chapter 3: Ge NC Ligand Exchange, Thin-Film Casting, and Electrical Conductivity Measurements

Introduction

Solution-phase synthesis of colloidal Ge nanocrystals (Ge NCs) has progressed significantly over the past two decades, but the surface chemistry of Ge NCs is underdeveloped and poorly understood compared to other semiconductor nanocrystal systems.[19] Understanding and controlling the surface of Ge NCs is essential for practical applications of Ge-based nanomaterials, so despite the readily available syntheses of Ge NCs, there is little practical use until the surface chemistry is better developed.

Nanomaterials are dimensionally confined in at least one direction, giving the material a high surface area to volume ratio. Compared to macroscale materials, a relatively high percentage of the atoms comprise the material surface (e.g. approximately 7% of the Ge atoms in a spherical 10 nm GeNC are surface atoms). These surface atoms are often bound to a heterogeneous atom or molecule, meaning that their coordination environment is different than that of the interior atoms of the NC. Consequently, the surface ligands influence the physical properties of the individual NCs and can significantly affect the physical transport properties of densely packed NC thin-films.[44,45] These effects have been well-documented for many semiconductor NC systems, but there are few examples that demonstrate surface ligand control over colloidal GeNCs or other Group-IV NC systems.[46–48] Thus, it is important to establish precise control over the NC surface ligands before the Ge NC system can be fully studied and understood, and subsequently used for the development of Ge NC-based solid state devices.

Progress Towards Ge NC Ligand Exchange

The synthesis of colloidal Ge NCs generally involves reduction of a germanium halide precursor in a high boiling point solvent, and the resulting Ge NCs are capped with a layer of the solvent molecules. These high boiling point solvents are typically long alkyl chains, meaning that the Ge NCs are insulated by a dense layer of long alkyl chains. This layer of nonpolar surface ligands lends colloidal stability and protects against oxidation and aggregation, but exchange of the surface ligands is desirable for many applications, particularly for the preparation of electrically conductive Ge NC thin films (**Figure 3.1**). Ge usually forms covalent bonds, unlike the more ionic II-VI, IV-VI, and III-V semiconductor systems, the modular surface chemistries of which have been extensively studied. Instead, the covalently bonded surface ligands require distinct chemical treatments to remove or replace them.

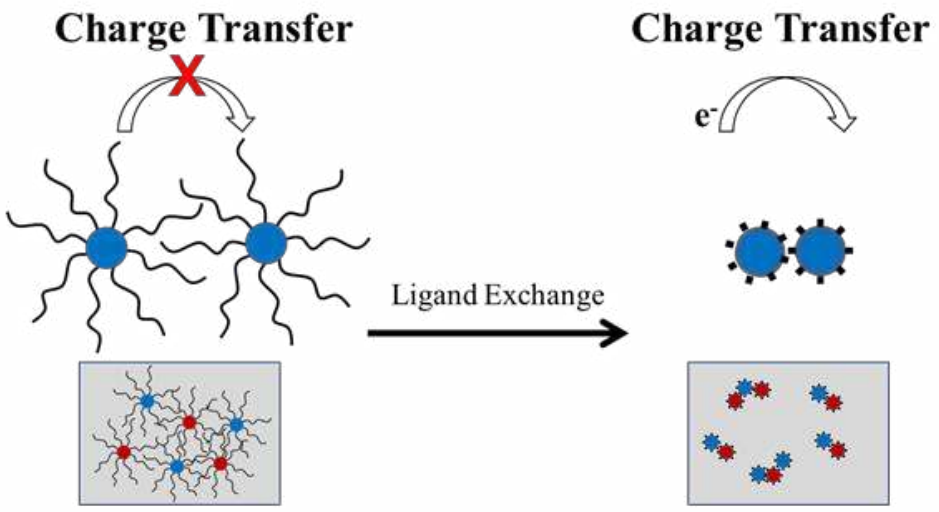

Figure 3.1: Ge NCs covered in long aliphatic surface ligands are too far apart for inter-particle charge transfer, preventing electrical conductivity in a NC thin film (Left). Ge NCs after removal of aliphatic ligands and replacement with short ligands, allowing denser NC packing and significantly improved electrical conductivity (Right).

Thermal reduction of GeX_2 and GeX_4 precursors using oleylamine (OAm) produces colloidally stable Ge NCs. This synthesis is high-yielding and produces fairly monodisperse Ge NCs, so it is commonly used to make Ge NCs, which are with capped OAm ligands. The OAm molecule ($C_{18}H_{35}NH_2$) is a long aliphatic chain and the terminal amine is suspected to be the group that coordinates to the GeNC surface. However, the nature of the OAm-GeNC surface interaction is poorly understood, which has hindered attempts to design rational methods for the exchange of OAm with other molecules.

There are few reports of colloidal Ge NC surface ligand exchange. Elemental sulfur and ammonium sulfide have been used to improve ligand exchange for OAm-capped Ge NCs and Ge/CdS core/shell NCs.[18,40] The role of sulfur in these examples is unclear, but it is hypothesized that the sulfur may reduce the Ge surface or even bind to the Ge surface, making the OAm more labile to exchange with shorter, polar ligands such as hydrazine or mercaptosuccinnic acid.[18,40,49]

The results in this Chapter describe the sulfur treatment of OAm-capped Ge NCs to facilitate exchange of the native OAm ligands with shorter ligands, specifically hydrazine (N_2H_4). Hydrazine is much shorter than OAm and significantly reduces the Ge NC interparticle spacing when the NCs are cast into a dense NC thin film. The sulfur treatment was modified to optimize ligand exchange with hydrazine and was then cast into NC thin films. Film casting methods were investigated and modified to improve the electrical conductivity. Ultimately, the hydrazine-capped Ge NCs were impractical for film casting applications, but electrical conductivity was significantly improved.

Experimental

General Procedures for Film-casting. Germanium nanocrystals (Ge NCs) were synthesized by heating 0.6 mmol $GeBr_2$ in 5 mL oleylamine (OAm) to 280° C for 2 hrs under

nitrogen. The OAm-capped Ge NCs were isolated and washed by centrifugation with three washes using a mixture of acetone, methanol, and ethanol. After the final wash, the Ge NCs were dispersed in toluene and stored in a nitrogen glovebox. For transfer to either hexane or DCM, the Ge NCs were precipitated from solution using MeOH, centrifuged, and re-dispersed in the desired solvent. Si substrates were used for film-casting and were prepared by plasma-cleaning and baking the substrates at 120° C before use. Substrates with pre-patterned Au electrodes were used for electrical conductivity measurements.

Sulfur-treatment of Ge NCs. Ge NCs were first synthesized and isolated, and aliquots of the synthesis were re-dispersed in 5 mL OAm under air-free conditions. The reaction was sealed and placed under positive nitrogen pressure on a Schlenk line. The reaction was heated to temperatures between 170 °C – 290 °C, and then various volumes of 0.1 M S_8 in OAm were slowly injected at the target temperature. The reaction remained at that temperature for 1 hr, and then the S-treated Ge NCs were washed three times using polar solvents and centrifugation, and finally stored in toluene in an air-free glovebox.

Solution-phase Ligand Exchange. OAm ligands were exchange with hydrazine ligands using a bi-phasic setup. The S-treated Ge NCs dispersed in toluene were added to a scintillation vial with a stir bar and 1.5 mL hydrazine was added. The mixture was stirred for 2 hrs, and then left for 10 min to allow the immiscible hydrazine and toluene to fully separate. The toluene layer was discarded, and 5 mL toluene was added and the solution was stirred for 10 min, after which the toluene was again discarded. After repeating this step twice, the Ge NCs dispersed in hydrazine were transferred to a clean vial, making sure to avoid transfer of any toluene.

Dip-coating OAm-capped Ge NCs. 230 °C S-treated OAm-capped Ge NCs were dispersed in 30 mL hexane and placed on a programmable dip-coating machine. Ligand exchange

solutions were prepared using acetonitrile or methanol to prepare 0.1 M solutions of ethylenediamine, hydrazine, or ammonium thiocyanate. Si substrates were first dipped into the NC solution, followed by a soak in the ligand exchange solution, followed by a rinse in acetonitrile. This cycle was repeated 21 times to build up a film of desired thickness. For certain trials, an intermediate baking step was introduced where the substrate was removed after a given number of cycles and baked on a 300 °C hot plate for 5 min.

Dip-coating CTAB-capped Ge NCs. S-treated CTAB-capped Ge NCs were dispersed in 30 mL DCM and placed on a programmable dip-coating machine. A saturated NaCl in MeOH solution was used as the ligand exchange solution. Si substrates were first dipped into the NC solution, followed by a soak in the NaCl solution, followed by a rinse in acetonitrile. This cycle was repeated 21x to build up a film of desired thickness.

Spin-casting Hzn-capped Ge NCs. Spin-cast films were produced from colloidal Ge NCs dispersed in hydrazine (Hzn). These solutions were spun on oxide-coated Si substrates and SiN substrates. After depositing 15 µL of the NC solution, the spin-coater was accelerated to 600 rpm until the hydrazine evaporated.

Drop-casting Hzn-capped Ge NCs. Drop-cast films were produced by placing 5 µL of the colloidal Ge NCs in Hzn onto Si substrates or devices. The temperature of the substrate was varied using a hot plate set to temperatures between room temperature and 125° C.

Characterization. Ligand exchange of Ge NC thin-films was characterized using FT-IR scans. The thickness and architecture of the film were evaluated using SEM imaging. Electrical conductivity was examined using a probe station in a nitrogen glovebox. The source-drain voltage was scanned from 50 V to -50 V, and the source-drain current was recorded.

Results and Discussion

Part 1: Sulfur-treatment and Solution-phase Ligand Exchange.

Ge NCs were treated with a S_8-OAm solution at 230 °C, consistent with literature procedures, and the S-treated Ge NCs were more amenable for ligand exchange with hydrazine (Hzn) than as-synthesized Ge NCs.[40] When Hzn was stirred with the S-treated Ge NCs, many of the particles migrated from the nonpolar toluene layer to the polar Hzn layer. In contrast, the as-synthesized Ge NCs mostly remained in the toluene, indicating that little or no OAm was replaced by Hzn (**Figure 3.2**). It was initially determined that the 230 °C S-treatment was acceptable for ligand exchange with Hzn, so dip-coating film preparation was explored, which is discussed in the next section. However, the S-treatment was revisited after the dip-coating film preparations failed.

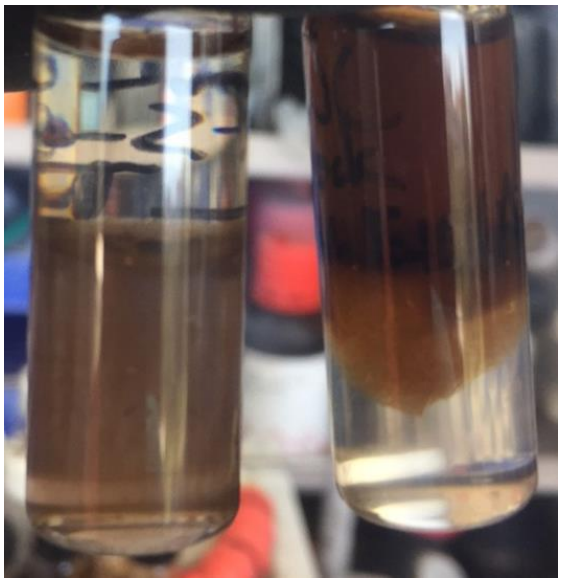

Figure 3.2: (Left) 230 °C S-treated Ge NCs and (Right) as-synthesized Ge NCs after stirring in toluene and hydrazine. The as-synthesized Ge NCs remained almost entirely in the toluene, while the S-treated Ge NCs migrated to the hydrazine.

After re-examining the S-treatment methods, it was determined that S-treatment at 230 °C did not improve ligand exchange as well as S-treatment at 260 °C. Even though the 230 °C S-treated Ge NCs were dispersible in Hzn, the solution was cloudy, indicative of aggregation, and unstable over time. Comparatively, the 260 °C S-treated Ge NCs produced an optically clear colloidal solution in Hzn (**Figure 3.3**). Furthermore, FT-IR scans of the S-treated Ge NCs dispersed in Hzn showed that the 230 °C S-treated sample still contained OAm on the particle surfaces, whereas the 260 °C S-treated sample did not show any evidence of OAm leftover after Hzn exchange (**Figure 3.4**).

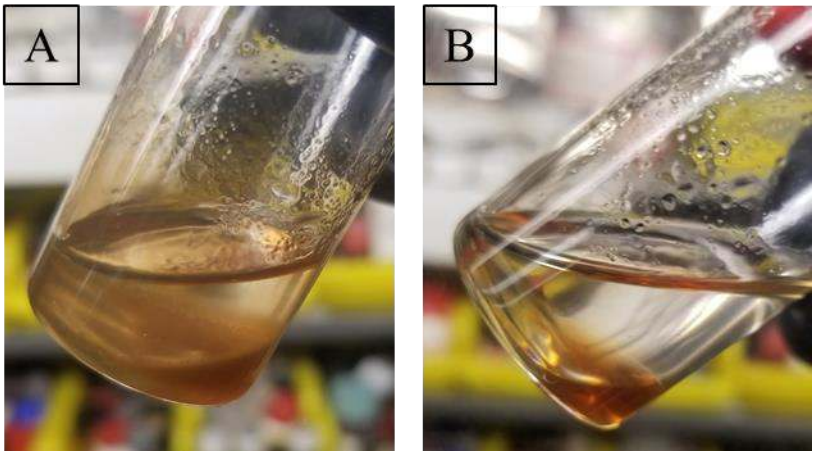

Figure 3.3: (A) 230 °C S-treated Ge NCs after Hzn ligand exchange, and (B) 260 °C S-treated Ge NCs after Hzn ligand exchange. The lack of cloudiness in the Hzn layer for the 260 °C S-treated Ge NCs shows improved Hzn ligand exchange compared to the 230 °C S-treated Ge NC sample.

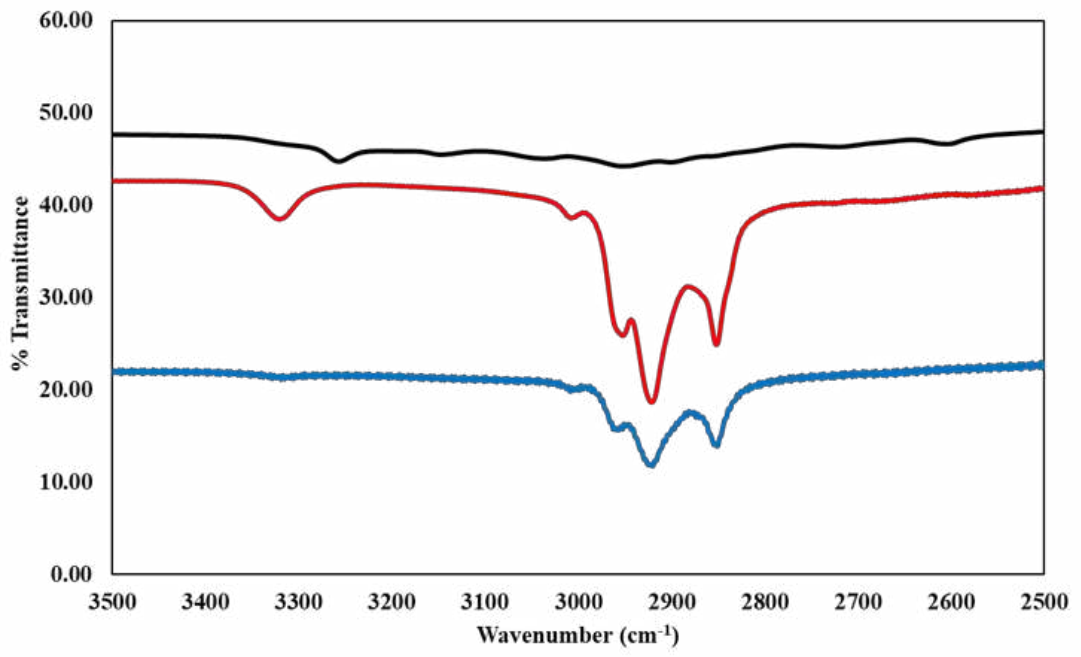

Figure 3.4: FT-IR scans of: (Red) OAm-capped Ge NCs before Hzn ligand exchange, showing clear presence of -CH_2 alkyl stretches; (Blue) Hzn-exchanged 230 °C S-treated Ge NCs, showing some alkyl stretches that indicate OAm was not completely removed and replaced by Hzn; (Black) Hzn-exchanged 260 °C S-treated Ge NCs showing little to no evidence of OAm after ligand exchange.

The role of the sulfur is not entirely understood, but it was determined to be essential for ligand exchange. Injection of excess S_8-OAm caused complete dissolution of the Ge NCs, indicated by the transition of the dark opaque brown color to a pale transparent yellow. The particle dissolution could be caused by formation of molecular germanium sulfide, driven by the thermodynamic stability of Ge-S bonds (551 kJ/mol).[19] It is possible that the Ge-S thermodynamics caused a layer of S to form on the Ge NCs, or alter the bonding between the OAm ligands and particle surface.[18,49]

Part 2: Dip-coating Ge NCs.

SEM images of dip-coated films revealed that the NC films were smooth and devoid of cracks (**Figure 3.5**). However, FT-IR scans showed that OAm ligands were not effectively removed from the NC thin film, and electrical conductivity measurements showed little or no conductivity, regardless of the ligand choice and number of dip-coating cycles.

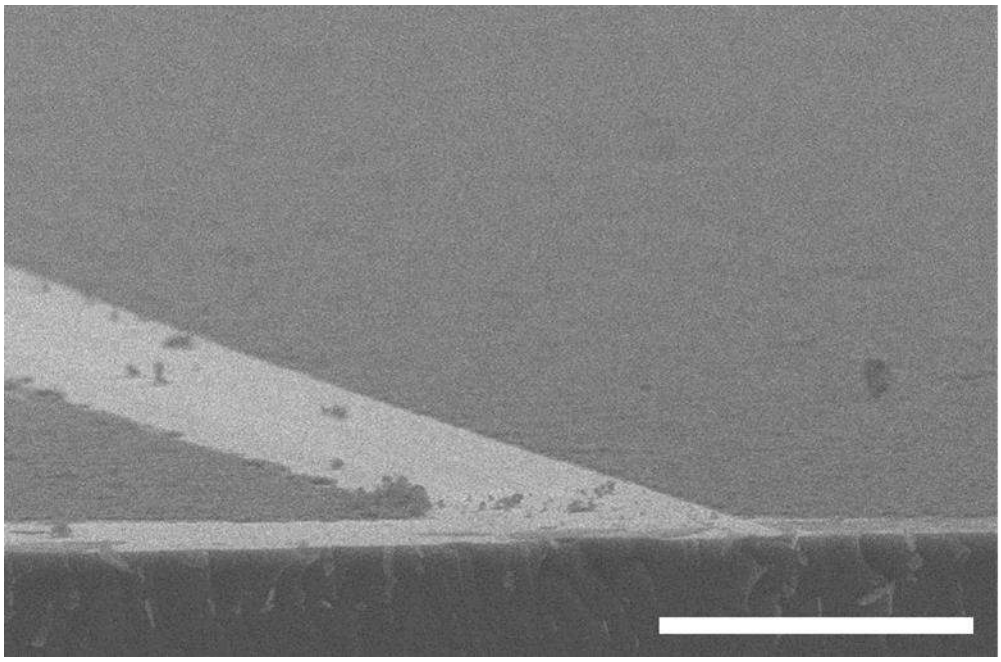

Figure 3.5: SEM image showing a smooth Ge NC assembled from dip-coating.

(Scale bar = 10 μm)

The poor electrical conductivity was attributed to incomplete removal of OAm ligands detected in FT-IR scans, and since OAm forms a strong bond with the Ge NC surface, cetyltrimethylammonium bromide (CTAB) was explored as a replacement for OAm. CTAB is ionic and cannot form covalent bonds with the Ge NC surface, so CTAB should theoretically be easier to remove from the NC surface.[18] First, S-treated OAm-capped Ge NCs were dispersed in DCM, and the solution was saturated with CTAB to drive replace of OAm with CTAB. The CTAB-coated Ge NCs were then used for similar dip-coating experiments, and a saturated NaCl

methanol solution was used for ligand exchange to maintain charge neutrality at the NC surface after CTAB removal.

SEM images showed smooth NC thin films, and individual Ge NCs were resolved (**Figure 3.6**). Previously, this was not possible due to charging in the NC films, and the ability to resolve individual NCs was encouraging since it suggested improved electrical conductivity. FT-IR scans and electrical conductivity measurements, however, revealed that the CTAB ligands were not fully removed and the films were not conductive (**Figure 3.7**).

Figure 3.6: Dip-coated NC film obtained from CTAB-capped Ge NCs and dipped into a NaCl MeOH solution. Individual Ge NCs are resolvable, indicating that charging within the film was dissipated. (Scale bar = 50 nm)

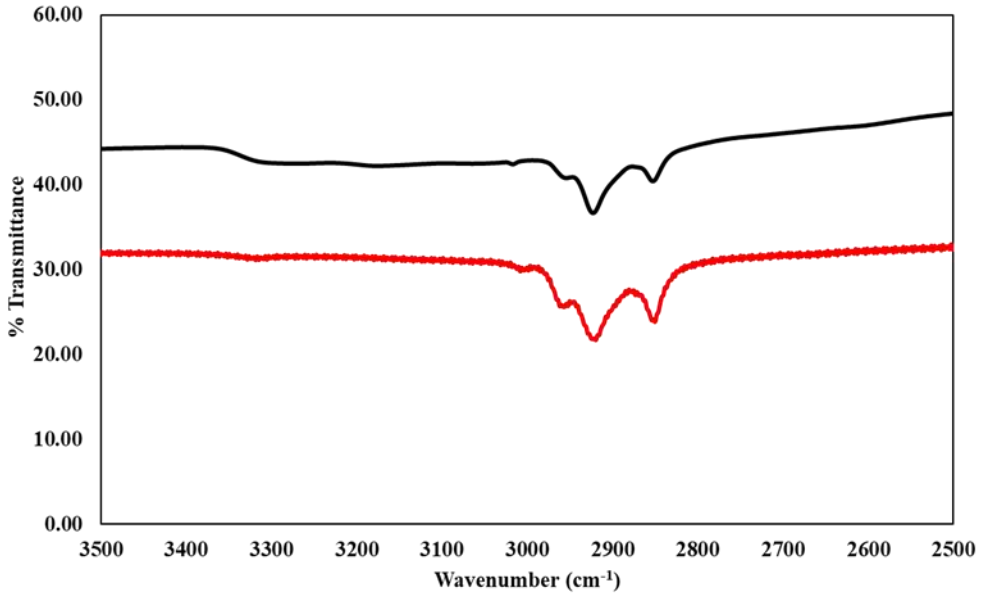

Figure 3.7: FT-IR scans of: (Black) Dip-coated film from CTAB-capped Ge NCs, (Red) CTAB-capped Ge NCs prior to dip-coating. Alkyl stretches are evident, indicating that significant amounts of CTAB remained in the dip-coated NC thin film.

Finally, intermediate baking steps were introduced into the dip-coating process with the goal of baking off the organic molecules in between each cycle of dip-coating. After a single cycle was completed, the substrates were placed on a hot plate set to 300° C. The substrates were heated for 5 min in between each dip-coating cycle. SEM images revealed that the films were cracked and pitted, likely an indication that organic molecules were being evaporated out of the film (**Figure 3.8**). Even with the intermediate baking steps, FT-IR scans indicated significant presence of CTAB, and electrical conductivity measurements produced results similar to the previous dip-coating results. The highest electrical conductivities were barely measurable, with resistance of 10-500 GΩ, a value consistent with literature reports.[20]

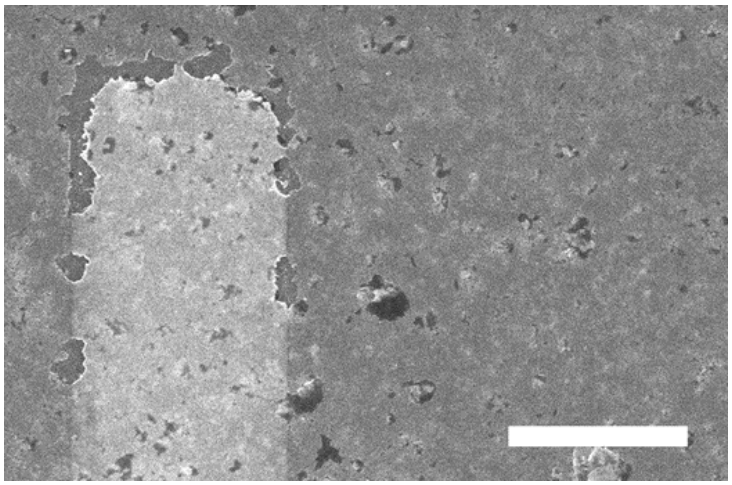

Figure 3.8: SEM image of a dip-coated thin film using CTAB-capped Ge NCs with intermediate baking steps. Pitting and cracking within the film indicated that organic molecules were likely being evaporated out the film (scale bar = 10 μm).

Part 3: Drop-cast and spun-cast from hydrazine-capped Ge NCs.

After reaching the apparent limitations of the dip-coating methods, the S-treatment of the Ge NCs was revisited, as described in Part 1 of this Chapter. FT-IR scans showed that all or almost all of the OAm was removed from the 260 °C S-treated Ge NCs (**Figure 3.4**). After ligand exchange with Hzn, the Ge NCs were dispersed in Hzn, but dip-coating was not possible with the Hzn-capped Ge NCs because Hzn solvent did not wet the surface of the substrates well. Dipping substrates into the Hzn-capped Ge NC solution produced no thin-films because the hydrazine was not volatile enough to evaporate and deposit NCs as the substrate was slowly raised out of the solution. Consequently, drop-casting and spin-casting were explored as alternatives.

Drop-casting the Hzn-capped Ge NCs onto Si substrates was the most practical method for film preparation and electrical conductivity measurements, since it ensured that the Ge NCs were deposited onto the substrate. The substrates were heated on a hot plate, and the temperature was varied to determine an optimal temperature for evaporation of the Hzn. Ultimately, this method

was impractical for electrical characterization because the film was not uniformly distributed across the Au electrodes, making it difficult to compare the conductivities of NC films cast at different temperatures. Nevertheless, the drop-cast films exhibited consistently measurable electrical conductivity, demonstrating that the Hzn-capped Ge NCs were amenable for producing electrically conductive Ge NC thin films

The difficulties encountered in dip-coating Hzn-capped Ge NCs were also obstacles to spin-casting the Hzn-capped Ge NCs. The hydrazine did not evaporate quickly and did not wet the Si substrate well enough to deposit Ge NCs onto the solid Si substrate, so most of the hydrazine flew off of the substrate, carrying the majority of the Ge NCs with it.

The Hzn wetted the surface of SiN substrates better than the surface of Si substrates, and Ge NC thin-films were successfully produced on the SiN substrates. SEM imaging revealed that these films were not very consistent (**Figure 3.9**). Despite the obstacles to film-casting, the Ge NC thin films exhibited good electrical conductivity, with resistance values approaching 1 MΩ · cm, exceeding existing literature values for Ge NC thin films cast from colloidal solutions (**Figure 3.10**).

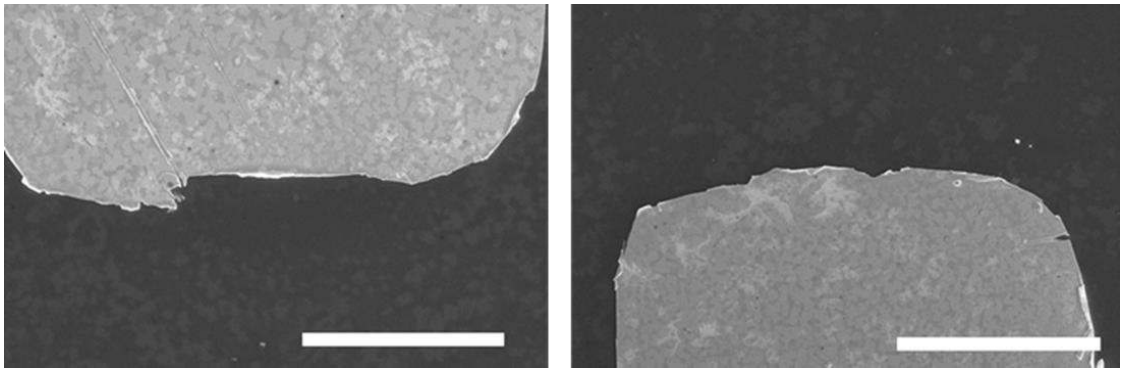

Figure 3.9: SEM images of spin-cast Ge NC thin films, cast from colloidal Ge NCs dispersed in Hzn (scale bar = 50 μm).

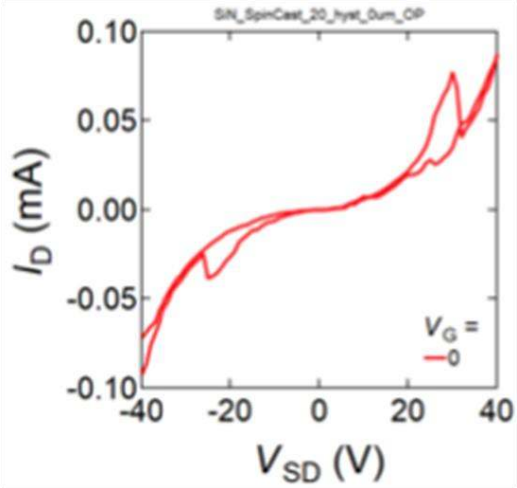

Figure 3.10: I-V curve of the spin-cast Ge NC thin film, imaged in **Figure 3.9**. The electrode geometry for this device was 230 µm x 115 µm.

Conclusions and Future Work

Strong interactions between the native OAm ligands and the Ge NC surface present an obstacle to electrically conductive bottom-up assembled Ge NC thin-films. While dip-coating methods produced uniform films, ligand exchange was limited and produced highly resistive films. Solution-phase ligand exchange with Hzn offers a route to conductive Ge NC thin-films, but the difficulties associated with deposition of Ge NCs from Hzn solvent complicate the characterization and control over the film thickness and morphology. Nevertheless, the spin-casted films from Hzn-capped Ge NCs exceeded electrical conductivities recorded in the literature and present a viable step towards electrically conductive thin-films that could be adapted for thermoelectric studies.

To produce more consistent thin films, the original dip-coating preparations should be revisited. The 230 °C S-treated Ge NCs were used in the original dip-coating experiments, but ligand exchange of 260 °C S-treated Ge NCs was improved, so the poor ligand exchange observed in the dip-coating thin films may be attributed to the inferior S-treatment conditions. If the dip-coating experiments with the 260 °C S-treated Ge NCs produces good thin films with improved

ligand exchange and electrical conductivity, then heterostructured M-Ge/Ge NC thin films should be assembled to begin investigation of the energy filtering TE effects outlined in Chapter 1.

References

(1) Vaughn, D. D.; Schaak, R. E. Synthesis, Properties and Applications of Colloidal Germanium and Germanium-Based Nanomaterials. *Chem. Soc. Rev.* **2013**, *42* (7), 2861–2879.

(2) Pillarisetty, R. Academic and Industry Research Progress in Germanium Nanodevices. *Nature* **2011**, *479* (7373), 324–328.

(3) Hekmatshoar, B.; Shahrjerdi, D.; Hopstaken, M.; Fogel, K.; Sadana, D. K. High-Efficiency Heterojunction Solar Cells on Crystalline Germanium Substrates. *Appl. Phys. Lett.* **2012**, *101* (3), 32102.

(4) Fan Jiyang; Chu Paul K. Group IV Nanoparticles: Synthesis, Properties, and Biological Applications. *Small* **2010**, *6* (19), 2080–2098.

(5) Kamata, Y. High-k/Ge MOSFETs for Future Nanoelectronics. *Mater. Today* **2008**, *11* (1), 30–38.

(6) EIA - Annual Energy Outlook 2018 https://www.eia.gov/outlooks/aeo/ (accessed Mar 23, 2018).

(7) Yee, S. K.; LeBlanc, S.; Goodson, K. E.; Dames, C. $ per W Metrics for Thermoelectric Power Generation: Beyond ZT. *Energy Environ. Sci.* **2013**, *6* (9), 2561–2571.

(8) LeBlanc, S.; Yee, S. K.; Scullin, M. L.; Dames, C.; Goodson, K. E. Material and Manufacturing Cost Considerations for Thermoelectrics. *Renew. Sustain. Energy Rev.* **2014**, *32*, 313–327.

(9) Snyder, G. J.; Toberer, E. S. Complex Thermoelectric Materials. *Nat. Mater.* **2008**, *7* (2), 105–114.

(10) Shakouri, A. Recent Developments in Semiconductor Thermoelectric Physics and Materials. *Annu. Rev. Mater. Res.* **2011**, *41* (1), 399–431.

(11) Dresselhaus, M. S.; Chen, G.; Tang, M. Y.; Yang, R. G.; Lee, H.; Wang, D. Z.; Ren, Z. F.; Fleurial, J.-P.; Gogna, P. New Directions for Low-Dimensional Thermoelectric Materials. *Adv. Mater.* **2007**, *19* (8), 1043–1053.

(12) Zide, J. M. O.; Vashaee, D.; Bian, Z. X.; Zeng, G.; Bowers, J. E.; Shakouri, A.; Gossard, A. C. Demonstration of Electron Filtering to Increase the Seebeck Coefficient in In0.53Ga0.47As/In0.53Ga0.28Al0.19As Superlattices. *Phys. Rev. B* **2006**, *74* (20), 205335.

(13) Touzelbaev, M. N.; Zhou, P.; Venkatasubramanian, R.; Goodson, K. E. Thermal Characterization of Bi2Te3/Sb2Te3 Superlattices. *J. Appl. Phys.* **2001**, *90* (2), 763–767.

(14) Luther, J. M.; Law, M.; Beard, M. C.; Song, Q.; Reese, M. O.; Ellingson, R. J.; Nozik, A. J. Schottky Solar Cells Based on Colloidal Nanocrystal Films. *Nano Lett.* **2008**, *8* (10), 3488–3492.

(15) Yu, B.; Zebarjadi, M.; Wang, H.; Lukas, K.; Wang, H.; Wang, D.; Opeil, C.; Dresselhaus, M.; Chen, G.; Ren, Z. Enhancement of Thermoelectric Properties by Modulation-Doping in Silicon Germanium Alloy Nanocomposites. *Nano Lett.* **2012**, *12* (4), 2077–2082.
(16) Joshi, G.; Lee, H.; Lan, Y.; Wang, X.; Zhu, G.; Wang, D.; Gould, R. W.; Cuff, D. C.; Tang, M. Y.; Dresselhaus, M. S.; et al. Enhanced Thermoelectric Figure-of-Merit in Nanostructured P-Type Silicon Germanium Bulk Alloys. *Nano Lett.* **2008**, *8* (12), 4670–4674.
(17) Vaughn II, D.; Sun, D.; Moyer, J. A.; Biacchi, A. J.; Misra, R.; Schiffer, P.; Schaak, R. E. Solution-Phase Synthesis and Magnetic Properties of Single-Crystal Iron Germanide Nanostructures. *Chem. Mater.* **2013**, *25* (21), 4396–4401.
(18) Wheeler, L. M.; Nichols, A. W.; Chernomordik, B. D.; Anderson, N. C.; Beard, M. C.; Neale, N. R. All-Inorganic Germanium Nanocrystal Films by Cationic Ligand Exchange. *Nano Lett.* **2016**, *16* (3), 1949–1954.
(19) Muthuswamy, E.; Zhao, J.; Tabatabaei, K.; Amador, M. M.; Holmes, M. A.; Osterloh, F. E.; Kauzlarich, S. M. Thiol-Capped Germanium Nanocrystals: Preparation and Evidence for Quantum Size Effects. *Chem. Mater.* **2014**, *26* (6), 2138–2146.
(20) Tabatabaei, K.; Lu, H.; Nolan, B. M.; Cen, X.; McCold, C. E.; Zhang, X.; Brutchey, R. L.; van Benthem, K.; Hihath, J.; Kauzlarich, S. M. Bismuth Doping of Germanium Nanocrystals through Colloidal Chemistry. *Chem. Mater.* **2017**, *29* (17), 7353–7363.
(21) Fredrick, S. J.; Prieto, A. L. Solution Synthesis and Reactivity of Colloidal Fe2GeS4: A Potential Candidate for Earth Abundant, Nanostructured Photovoltaics. *J. Am. Chem. Soc.* **2013**, *135* (49), 18256–18259.
(22) Xue, D.-J.; Wang, J.-J.; Wang, Y.-Q.; Xin, S.; Guo, Y.-G.; Wan, L.-J. Facile Synthesis of Germanium Nanocrystals and Their Application in Organic–Inorganic Hybrid Photodetectors. *Adv. Mater.* **2011**, *23* (32), 3704–3707.
(23) Boote, B. W.; Men, L.; Andaraarachchi, H. P.; Bhattacharjee, U.; Petrich, J. W.; Vela, J.; Smith, E. A. Germanium–Tin/Cadmium Sulfide Core/Shell Nanocrystals with Enhanced Near-Infrared Photoluminescence. *Chem. Mater.* **2017**, *29* (14), 6012–6021.
(24) Muthuswamy, E.; Iskandar, A. S.; Amador, M. M.; Kauzlarich, S. M. Facile Synthesis of Germanium Nanoparticles with Size Control: Microwave versus Conventional Heating. *Chem. Mater.* **2013**, *25* (8), 1416–1422.
(25) Spann, J. Y.; Anderson, R. A.; Thornton, T. J.; Harris, G.; Thomas, S. G.; Tracy, C. Characterization of Nickel Germanide Thin Films for Use as

Contacts to P-Channel Germanium MOSFETs. *IEEE Electron Device Lett.* **2005**, *26* (3), 151–153.
(26) Grzela, T.; Capellini, G.; Koczorowski, W.; Schubert, M. A.; Czajka, R.; Curson, N. J.; Heidmann, I.; Schmidt, T.; Falta, J.; Schroeder, T. Growth and Evolution of Nickel Germanide Nanostructures on Ge(001). *Nanotechnology* **2015**, *26* (38), 385701.
(27) Zhang, G.; Zhang, Y.-W. Strain Effects on Thermoelectric Properties of Two-Dimensional Materials. *Mech. Mater.* **2015**, *Part 2* (91), 382–398.
(28) Dellas, N. S.; Minassian, S.; Redwing, J. M.; Mohney, S. E. Formation of Nickel Germanide Contacts to Ge Nanowires. *Appl. Phys. Lett.* **2010**, *97* (26), 263116.
(29) Goley, P. S.; Hudait, M. K. Germanium Based Field-Effect Transistors: Challenges and Opportunities. *Materials* **2014**, *7* (3), 2301–2339.
(30) Ruddy, D. A.; Johnson, J. C.; Smith, E. R.; Neale, N. R. Size and Bandgap Control in the Solution-Phase Synthesis of Near-Infrared-Emitting Germanium Nanocrystals. *ACS Nano* **2010**, *4* (12), 7459–7466.
(31) Wu, J.; Sun, Y.; Zou, R.; Song, G.; Chen, Z.; Wang, C.; Hu, J. One-Step Aqueous Solution Synthesis of Ge Nanocrystals from GeO 2 Powders. *CrystEngComm* **2011**, *13* (11), 3674–3677.
(32) Zaitseva, N.; Dai, Z. R.; Grant, C. D.; Harper, J.; Saw, C. Germanium Nanocrystals Synthesized in High-Boiling-Point Organic Solvents. *Chem. Mater.* **2007**, *19* (21), 5174–5178.
(33) Gerion, D.; Zaitseva, N.; Saw, C.; Casula, M. F.; Fakra, S.; Van Buuren, T.; Galli, G. Solution Synthesis of Germanium Nanocrystals: Success and Open Challenges. *Nano Lett.* **2004**, *4* (4), 597–602.
(34) Esteves, R. J. A.; Ho, M. Q.; Arachchige, I. U. Nanocrystalline Group IV Alloy Semiconductors: Synthesis and Characterization of Ge1–xSnx Quantum Dots for Tunable Bandgaps. *Chem. Mater.* **2015**, *27* (5), 1559–1568.
(35) Ramasamy, K.; Kotula, P. G.; Fidler, A. F.; Brumbach, M. T.; Pietryga, J. M.; Ivanov, S. A. SnxGe1–x Alloy Nanocrystals: A First Step toward Solution-Processed Group IV Photovoltaics. *Chem. Mater.* **2015**, *27* (13), 4640–4649.
(36) Buck, M. R.; Sines, I. T.; Schaak, R. E. Liquid-Phase Synthesis of Uniform Cube-Shaped GeTe Microcrystals. *Chem. Mater.* **2010**, *22* (10), 3236–3240.
(37) Vaughn II, D. D.; Patel, R. J.; Hickner, M. A.; Schaak, R. E. Single-Crystal Colloidal Nanosheets of GeS and GeSe. *J. Am. Chem. Soc.* **2010**, *132* (43), 15170–15172.

(38) Vaughn, D.; Sun, D.; Levin, S. M.; Biacchi, A. J.; Mayer, T. S.; Schaak, R. E. Colloidal Synthesis and Electrical Properties of GeSe Nanobelts. *Chem. Mater.* **2012**, *24* (18), 3643–3649.
(39) Xue, D.-J.; Tan, J.; Hu, J.-S.; Hu, W.; Guo, Y.-G.; Wan, L.-J. Anisotropic Photoresponse Properties of Single Micrometer-Sized GeSe Nanosheet. *Adv. Mater.* **2012**, *24* (33), 4528–4533.
(40) Guo, Y.; Rowland, C. E.; Schaller, R. D.; Vela, J. Near-Infrared Photoluminescence Enhancement in Ge/CdS and Ge/ZnS Core/Shell Nanocrystals: Utilizing IV/II–VI Semiconductor Epitaxy. *ACS Nano* **2014**, *8* (8), 8334–8343.
(41) Bondi, J. F.; Misra, R.; Ke, X.; Sines, I. T.; Schiffer, P.; Schaak, R. E. Optimized Synthesis and Magnetic Properties of Intermetallic Au3Fe1−x, Au3Co1−x, and Au3Ni1−x Nanoparticles. *Chem. Mater.* **2010**, *22* (13), 3988–3994.
(42) Cosentino, S.; Torrisi, G.; Raciti, R.; Zimbone, M.; Crupi, I.; Mirabella, S.; Terrasi, A. Growth Kinetics of Colloidal Ge Nanocrystals for Light Harvesters. *RSC Adv.* **2016**, *6* (44), 38454–38462.
(43) Gao, Y.; Peng, X. Crystal Structure Control of CdSe Nanocrystals in Growth and Nucleation: Dominating Effects of Surface versus Interior Structure. *J. Am. Chem. Soc.* **2014**, *136* (18), 6724–6732.
(44) Liu, Y.; Gibbs, M.; Puthussery, J.; Gaik, S.; Ihly, R.; Hillhouse, H. W.; Law, M. Dependence of Carrier Mobility on Nanocrystal Size and Ligand Length in PbSe Nanocrystal Solids. *Nano Lett.* **2010**, *10* (5), 1960–1969.
(45) Liu, M.; Ma, Y.; Wang, R. Y. Modifying Thermal Transport in Colloidal Nanocrystal Solids with Surface Chemistry. *ACS Nano* **2015**, *9* (12), 12079–12087.
(46) Lynch, J.; Kotiuga, M.; Doan-Nguyen, V. V. T.; Queen, W. L.; Forster, J. D.; Schlitz, R. A.; Murray, C. B.; Neaton, J. B.; Chabinyc, M. L.; Urban, J. J. Ligand Coupling Symmetry Correlates with Thermopower Enhancement in Small-Molecule/Nanocrystal Hybrid Materials. *ACS Nano* **2014**, *8* (10), 10528–10536.
(47) Cho Eun Seon; Coates Nelson E.; Forster Jason D.; Ruminski Anne M.; Russ Boris; Sahu Ayaskanta; Su Norman C.; Yang Fan; Urban Jeffrey J. Engineering Synergy: Energy and Mass Transport in Hybrid Nanomaterials. *Adv. Mater.* **2015**, *27* (38), 5744–5752.
(48) Coates, N. E.; Yee, S. K.; McCulloch, B.; See, K. C.; Majumdar, A.; Segalman, R. A.; Urban, J. J. Effect of Interfacial Properties on Polymer–Nanocrystal Thermoelectric Transport. *Adv. Mater.* **2013**, *25* (11), 1629–1633.

(49) Kerr, A. T.; Placencia, D.; Gay, M. E.; Boercker, J. E.; Soto, D.; Davis, M. H.; Banek, N. A.; Foos, E. E. Sulfur-Capped Germanium Nanocrystals: Facile Inorganic Ligand Exchange. *J. Phys. Chem. C* **2017**, *121* (41), 22597–22606.